

UNIVERSITY OF OKLAHOMA

GRADUATE COLLEGE

THE IMPACT OF THERMALLY FORCED, NONPERIODIC
INTERNAL GRAVITY WAVES ON CONVECTIVE DEVELOPMENT

A THESIS

SUBMITTED TO THE GRADUATE FACULTY

in partial fulfillment of the requirements for the

degree of

MASTER OF SCIENCE

By

DANIEL LEE WEEKLEY

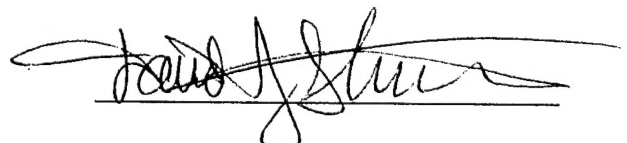
Norman, Oklahoma


2001

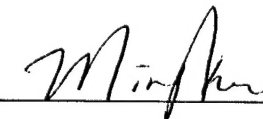
THE IMPACT OF THERMALLY FORCED, NONPERIODIC
INTERNAL GRAVITY WAVES ON CONVECTIVE DEVELOPMENT

A THESIS APPROVED FOR THE SCHOOL OF METEOROLOGY

BY



David J. Steiner


David J. Steiner


David J. Steiner

The views expressed in this article are those of the author and do not reflect the official policy or position of the United States Air Force, Department of Defense, or the U.S. Government

ACKNOWLEDGEMENTS

I am grateful to the countless number of people who selflessly contributed their time and expertise to ensure my scholastic and professional development during the pursuit of my Masters degree. Most notably, I would like to thank Dr. David J. Stensrud for his continued support throughout this endeavor. He has the ability to provide expert guidance in every phase of research, and yet he still gives enough freedom to allow one to explore new possibilities and take their research in unforeseen directions. In addition to the tangibles, he has provided me with a template of the consummate professional. His technical expertise, integrity, and willingness to put the needs of those who depend upon him in front of his own are just a few examples of how he personifies leadership.

A special thanks goes to Dr. Alan M. Shapiro and Dr. Ming Xue for their willingness to lend their expertise in the resolution of some difficult meteorological concepts. Their ability to effectively clarify the confusing is a trait that is held by very few.

I would also like to thank the staff of the OU School of Meteorology. I was always able to focus on research knowing that they

would be there to continually orchestrate the administrative aspect of my life at OU.

The National Severe Storms Laboratory deserves a special thanks for the use of its facilities and computer resources, without which this research would not have been possible.

Most importantly, I would like to thank my wife Although gainfully employed by the Air Force and actively completing her degree during this time, she always seemed to shoulder the bulk of parental responsibilities. The sacrifices made in the pursuit of my degree all seemed to be made by her.

Lastly, I thank the Air Force Institute of Technology Civilian Institution Programs for providing me this educational opportunity.

TABLE OF CONTENTS

ABSTRACT	vii
1. INTRODUCTION	1
1.1 Observed Thermal Forcing Profiles	4
1.2 Numerically Simulated Thermal Forcing Profiles	8
1.3 Buoyancy Bores	10
1.4 Motivation and Objectives	12
2. METHODS AND PROCEDURES	15
2.1 Model Description	15
2.2 Selection of Initial and Boundary Conditions	18
2.3 Simulation Procedures	18
2.4 Thermal Forcing Profile	22
3. MODEL GENERATED BUOYANCY BORES	26
3.1 Identification/Recognition of Buoyancy Bores	26
3.2 Thermal Forcing Dependence	30
3.3 Bore Interactions Between Thermal Forcing Regions	35
3.4 Grid Scale Dependence	38
3.5 The "Inverse-Bore"	40
3.6 The Advection of Convective Heating Regions	43
4. BORE BEHAVIOR IN A CONVECTIVE OUTBREAK	48
4.1 Developing the Convective Simulation	50
4.2 Behavior in an Area Separating Neighboring MCSs	53
4.3 Behavior in an Area Further Removed From MCSs	59
5. CONCLUSIONS	64
5.1 Additional Considerations	66
6. REFERENCES	69

ABSTRACT

The thermal forcing in the upper troposphere resulting from deep convection produces internal gravity-wave like disturbances called buoyancy bores. Although they propagate in a manner similar to gravity waves, their structure in time and space is nonperiodic; they travel as a pulse, propagating radially in all directions from the source of thermal forcing. The passage of these bores through the troposphere causes vertical displacements throughout the column in which they occupy. The actual displacements depend upon the vertical structure, or mode, of the bore. Some bores cause local subsidence, while other bores are characterized low-level ascent and upper-level subsidence. Based upon idealized simulations, theories about the contribution of bores to the suppression or enhancement of convection differ. One holds that bores are capable of suppressing convection away from a mesoscale convective system (MCS) while another holds that low-level convergence is supported by bores near an MCS.

This paper investigates buoyancy bore behavior in a mesoscale model simulation using initial and boundary conditions from an actual convective outbreak in the central plains of the United States. Despite low-level forcing produced by colliding outflow boundaries on this day, convection failed to initiate between two MCSs due to mid- to upper-level subsidence. Through manipulation of the convective parameterization scheme within the model, the initiation and suppression of convective heating regions is explicitly controlled. This technique of manual convective initiation allows for a better isolation of the specific sources of

thermal forcing. Once the behavioral characteristics of buoyancy bores are ascertained, an analysis of buoyancy bore behavior during the simulated convective outbreak is conducted.

The bores suspected of enhancing low-level convergence near MCSs never manifest themselves in the simulations. An anomalous feature, termed an inverse-bore, disrupts the normal low-level flow field between bores, inhibiting the normal development of these convergence-enhancing bores.

Examination of the simulated outbreak shows that the bores responsible for subsidence are confined to the upper troposphere and are stronger at the level of greatest thermal forcing. Even though these bores can produce sufficient localized subsidence to modify the tropospheric profile of temperature and dewpoint, they appear to form too high in the troposphere to produce modifications in atmospheric structure much below 600 hPa.

CHAPTER 1 - INTRODUCTION

The collision of cool outflow boundaries from neighboring mesoscale convective systems (MCSs) often results in significant low-level forcing for new convection. In addition, the most intense convective phase of these systems are often associated with the merging of mesoscale outflow boundaries (Knupp et al. 1998). In a conditionally unstable environment, there are cases where this boundary interaction appears to be sufficient to initiate convection between the two systems. However, even though an analysis of the low-level forcing and atmospheric stability may suggest an extremely high probability of initiating convection, the results are not always as expected, as revealed by Stensrud and Maddox (1988). Their analysis of soundings from a convective outbreak on 23-24 June 1985 reveals strong mid-level descending motions between two neighboring MCSs over a layer from 800 to 400 hPa. This subsidence is sufficient to maintain a capping inversion, thereby inhibiting the development of new convection despite strong low-level forcing from colliding outflows. They suggest that the convergence of upper-level outflows from the two systems is responsible for the mid- to upper-level subsidence (Fig. 1). While this is one mechanism by which subsidence can be generated between MCSs, it is by no means the only possibility.

In an examination of a similar squall-line gap on 14-15 June 1985, Johnson et al. (1995) propose that gravity-wave induced subsidence aloft alone is capable of preventing deep convection in opposition to low-level forcing. They suggest that vertical heating profiles representative of those found in MCSs produce these thermally forced gravity-wave like features, as shown by Nicholls et al. (1991a).

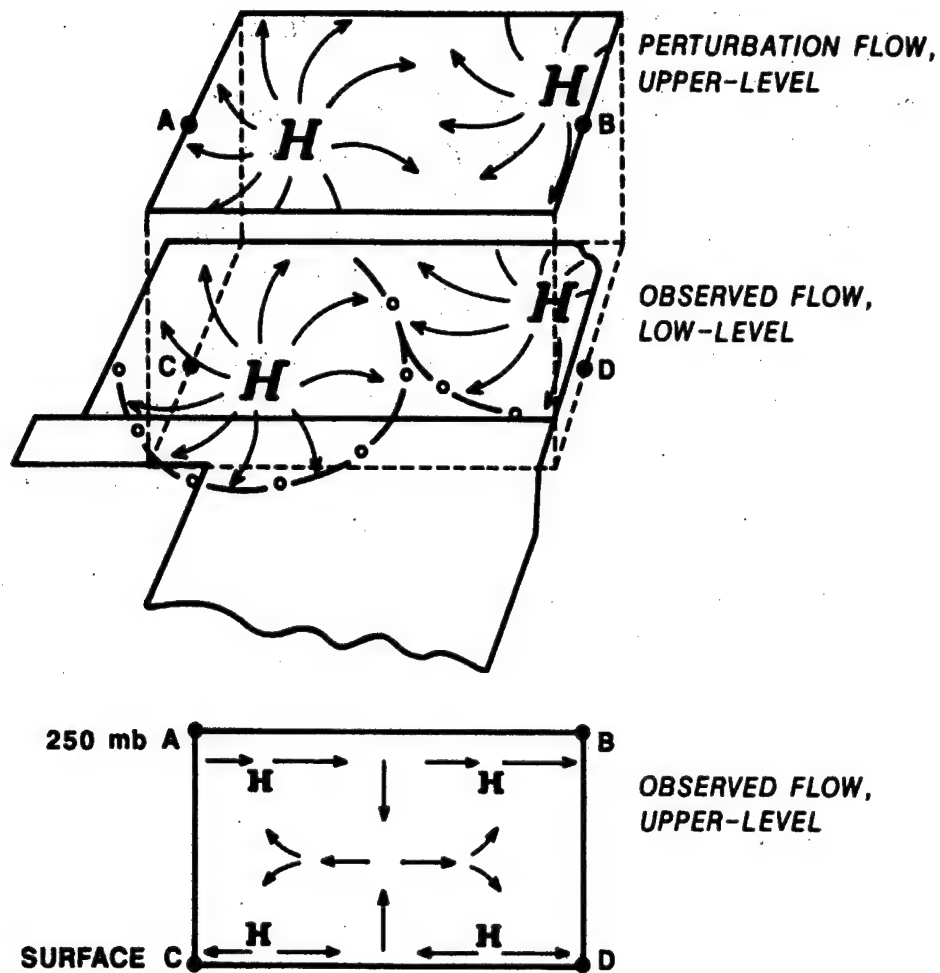


Fig. 1. Depiction of hypothesized mesoscale circulations showing observed low-level colliding outflows and the perturbation upper-level converging anticyclonic outflows. Lower portion of figure depicts hypothesized vertical circulations driven by the convergence of both the low-level and upper-level outflows in a vertical cross section specified by points a, b, c and d (from Stensrud and Maddox 1988).

These features are capable of producing local subsidence away from the parent convection (Nicholls et al. 1991a).

The term buoyancy bore refers to an internal gravity-wave like disturbance whose passage results in vertical displacements in a stratified fluid (Mapes 1993). Although they propagate in a manner similar to gravity waves, their structure in time and space is non-periodic; they travel as a pulse, propagating radially in all directions from the source of thermal forcing. In the atmosphere, these buoyancy bores (referred to as just “bores” in the remainder of this paper) are generated in response to thermal forcing resulting from convection. There are many different modes of bores, as identified by their vertical structure, each propagating at a different speed and demonstrating different properties (Nicholls et al. 1991a; Mapes 1993). The subsidence described by Johnson et al. (1995) is in response to one such bore structure, or mode.

Satellite data show that cloud clusters over tropical waters often occur in larger, tangled clusters. To explain this gregarious behavior of tropical convection, Mapes (1993) submits that there are bores capable of providing sufficient low-level adiabatic upward displacements to enhance, if not initiate, additional convection in the vicinity of MCSs.

The studies of Nicholls et al. (1991a) and Mapes (1993) seem to make very different conclusions. The first suggests that bores suppress convection. The other introduces the notion that bores can initiate convection. This is not a contradiction; the two different behaviors can coexist (Pandya and Durran 1996). This is because the bore mode referenced by Nicholls et al. (1991a) propagates at roughly twice the

speed as the bore mode highlighted by Mapes (1993). The specifics about bore behavior are discussed later, but it is important to note that the initiation of a bore is, in part, a function of the vertical profile of the thermal forcing (Mapes 1993). This dependency may explain the very different conclusions reached.

1.1. Observed Thermal Forcing Profiles

There are many differences in the environmental conditions of midlatitude mesoscale convective complexes (MCCs) or squall lines and the cloud clusters found in the Tropics. These differences are revealed by Wu (1993) in an analysis of the environmental conditions obtained from two separate experiments: The Oklahoma-Kansas Preliminary Regional Experiment for STORM-Central, studying the cumulus-environment interaction in midlatitude MCSs, and the GARP Atlantic Tropical Experiment, studying tropical MCSs. Generally, the large-scale forcing, vertical wind shear, and moist convective instability in tropical cloud clusters prove to be smaller than in midlatitude MCCs and squall lines. Yet the observed heat and moisture budget residuals show that the manner in which cumulus convection modifies the thermodynamic field is basically the same in the midlatitudes and tropics, and cumulus convection is the dominant process for thermodynamic modification of these environments. These similarities lead to similar vertical distributions of cumulus heating (Fig. 2). Although tropical convection yields a broader and weaker vertical distribution of heat than the midlatitude version, they both show a tendency to maximize the heating near 400 hPa. Considering this similarity, it is not unreasonable to conclude that the vertical distribution of thermal

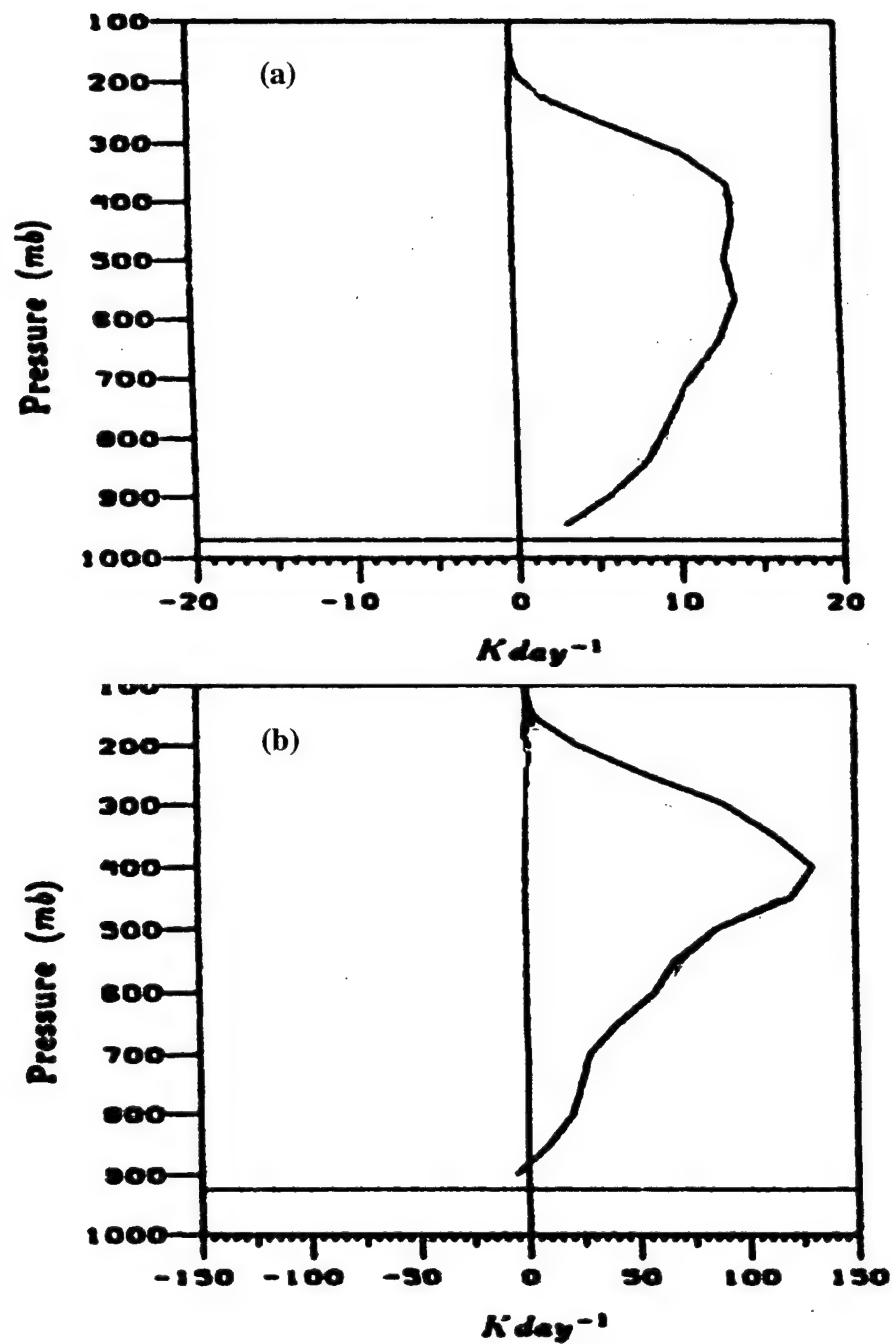


Fig. 2. Vertical profiles of heating resulting from cumulus convection in the (a) tropics and (b) midlatitudes (adapted from Wu 1993).

forcing in tropical cloud clusters may at times prove to be representative of what might be seen in midlatitude systems. Therefore, the examination of thermal forcing found in weakly sheared tropical cloud clusters may yield some insight into the thermal forcing profile one might expect from a convective system initiating in the mid-latitude environment examined in this paper.

Tropical convective clusters are characterized by groups of convective towers with extensive anvil clouds separated by regions of active stratiform clouds. Through an examination of rawinsonde data surrounding MCSs over the South China Sea, Johnson and Young (1983) construct profiles of the atmospheric heating that take place within these convective clusters (Fig. 3a). The heating in the mid- to upper-troposphere is a result of the latent heat release accompanying condensation and freezing of precipitation in both the convective towers and stratiform clouds. The cooling found in the lower levels of the atmosphere is characteristic of squall line stratiform regions (Haertel and Johnson 1999), whereas the cooling aloft is a result of overshooting tops protruding into the stratosphere. This profile is not unlike what is seen in midlatitude convective systems (Gallus and Johnson 1991). This is not surprising given that in the midlatitudes, MCSs are also characterized by a combination of deep convective cells surrounded by stratiform clouds (Ogura and Liou 1980).

In contrast to the approach taken by Johnson and Young (1983), Houze (1982) conducts a more numerical examination of the sensible heat budget associated with these types of clouds. By modeling idealized, tropical convective cloud clusters,

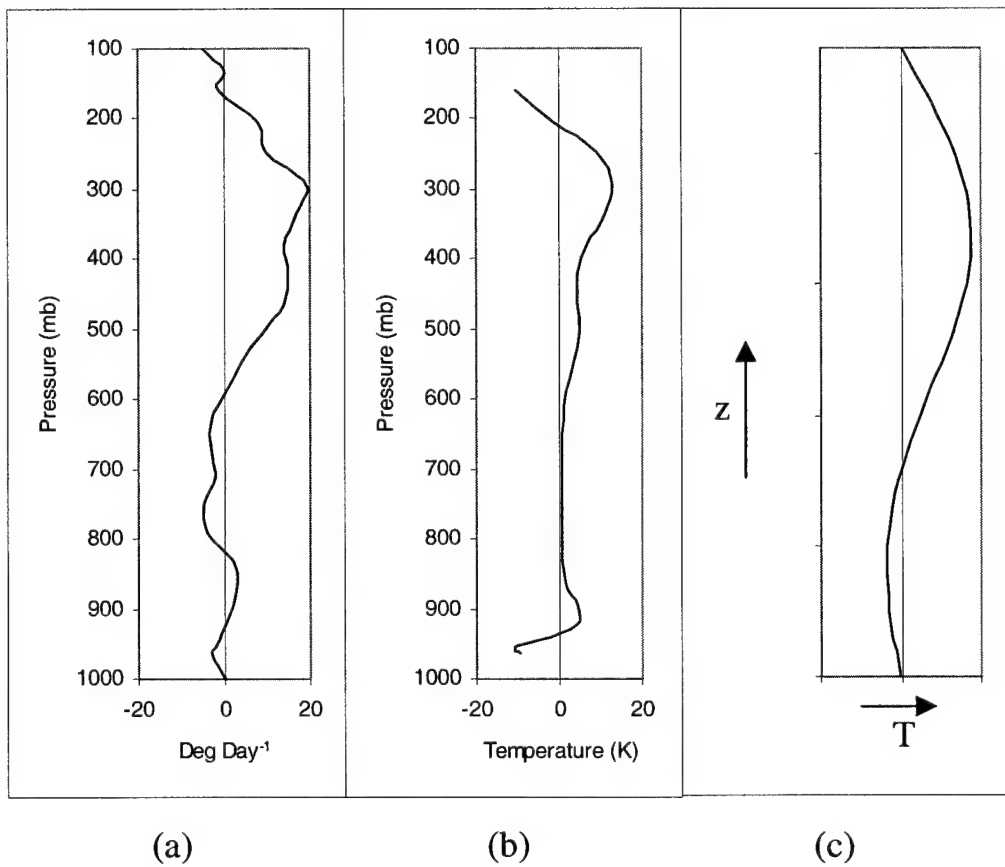


Fig. 3. Vertical profile of (a) atmospheric heating due to convection in the tropics, (adapted from Johnson and Young 1983, Fig. 4), (b) thermal forcing generated by the Kain-Fritsch convective parameterization scheme, and (c) thermal forcing analytically derived by summing convective and stratiform effects (adapted from Nicholls et al. 1991b, Fig. 4).

comprised of isolated deep convective cells connected by a widespread stratiform cloud shield, a similar heating profile is created. This type of heating profile can produce a variety of different buoyancy bore modes (Nicholls et al. 1991a).

1.2. Numerically Simulated Thermal Forcing Profiles

In an investigation of the atmospheric response to heating profiles that are characteristic of the convective and stratiform regions of squall lines, Nicholls et al. (1991a) consider the aforementioned vertical profile of thermal forcing (Fig. 3a). In an attempt to artificially reproduce an approximation of this thermal forcing profile, they choose to specify a thermal forcing of the form

$$Q = Q_0 \left(\frac{a^2}{x^2 + a^2} \right) \sin(lz) , \quad (1)$$

where Q_0 is the magnitude of thermal forcing, a is the horizontal half-width, $l = n\pi/H$ is the vertical wavenumber and H is the depth of the thermal forcing (taken to be 10 km). The goal is to use (1) to describe the observed heating profiles of both the deep convective and stratiform components of MCSs. Thus, the upper-tropospheric heating due to deep convection is most easily portrayed as a vertically oriented half-sine wave. To represent the stratiform contribution to the thermal forcing, a vertically oriented full-sine wave, with heating aloft and cooling below, is a reasonable choice. By superimposing the two waves, a thermal profile maximizing heating in the upper-levels, while also containing cooling in the low levels, is created (Fig. 4). Although the use of just two sine waves makes it difficult to accurately portray the shallowness

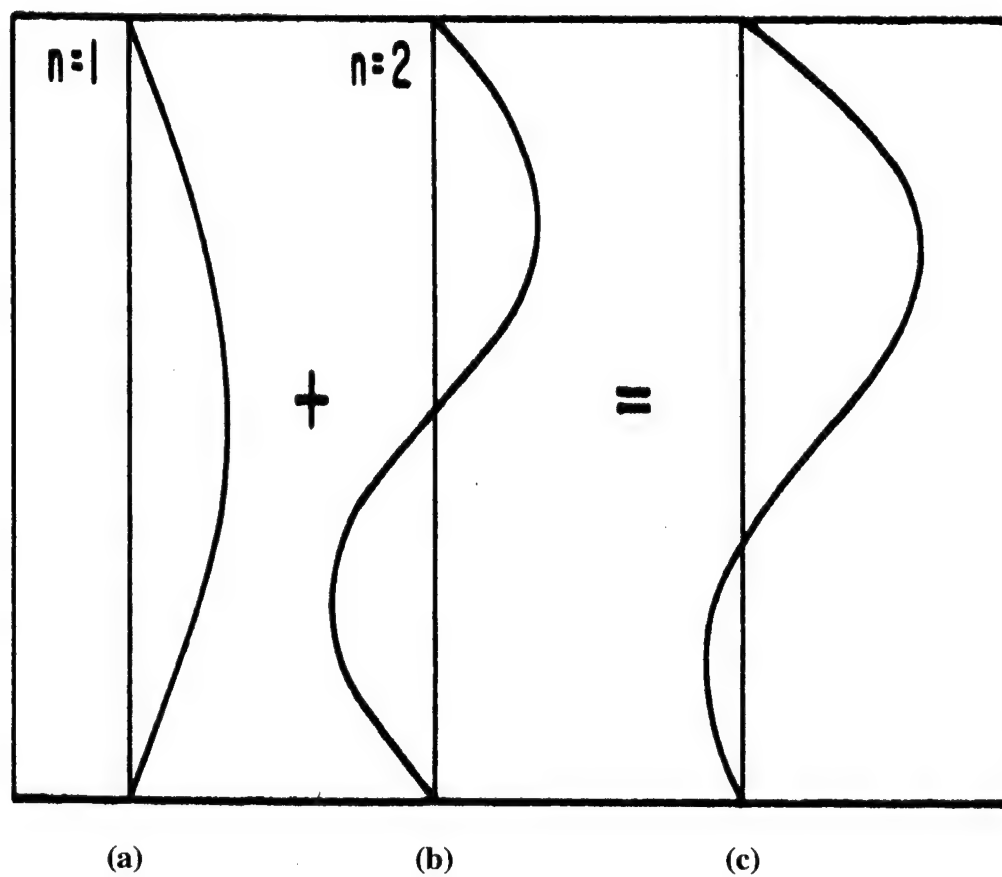


Fig. 4. Vertical distribution of the thermal forcing for (a) $n=1$ and (b) $n=2$ and (c) their sum. The magnitude of the thermal forcing is the same for each mode, positive for $n=1$, negative for $n=2$ (from Nicholls et al. 1991a).

of the surface cool layer sometimes observed (Fig. 3a and 3b), the overall heating profile is a good approximation to those observed in many convective systems.

Substituting the definition of the vertical wavenumber back into (1) we get a clearer picture of how the shape term in (1), namely

$$\sin\left(\frac{n\pi z}{H}\right), \quad (2)$$

is a function of the mode- n of the wave. Therefore, to represent different thermal forcing profiles, or shapes, different combinations of wave modes may be needed.

1.3. Buoyancy Bores

Applying a simple superposition of the $n = 1$ and $n = 2$ profiles of thermal forcing to a constantly stratified fluid at rest, Nicholls et al. (1991a) observe two distinct vertical modes of thermally forced gravity waves (Fig. 5). The different modes can be identified because they propagate away from the heat source at different speeds. The propagation speed is found to be

$$c = \frac{NH}{n\pi}, \quad (3)$$

where n is the vertical wave number of the thermal forcing (mode-1, mode-2, etc.) and N is the Brunt-Väisälä frequency.

The fast moving $n = 1$ mode is characterized by subsidence warming throughout the column it occupies. Aloft, flow is away from the heat source toward this mode-1 bore. At the surface, flow is toward the heat source from the bore (Fig. 5a). The $n = 2$ mode, traveling at half the speed of the mode-1 bore, produces ascent in the low

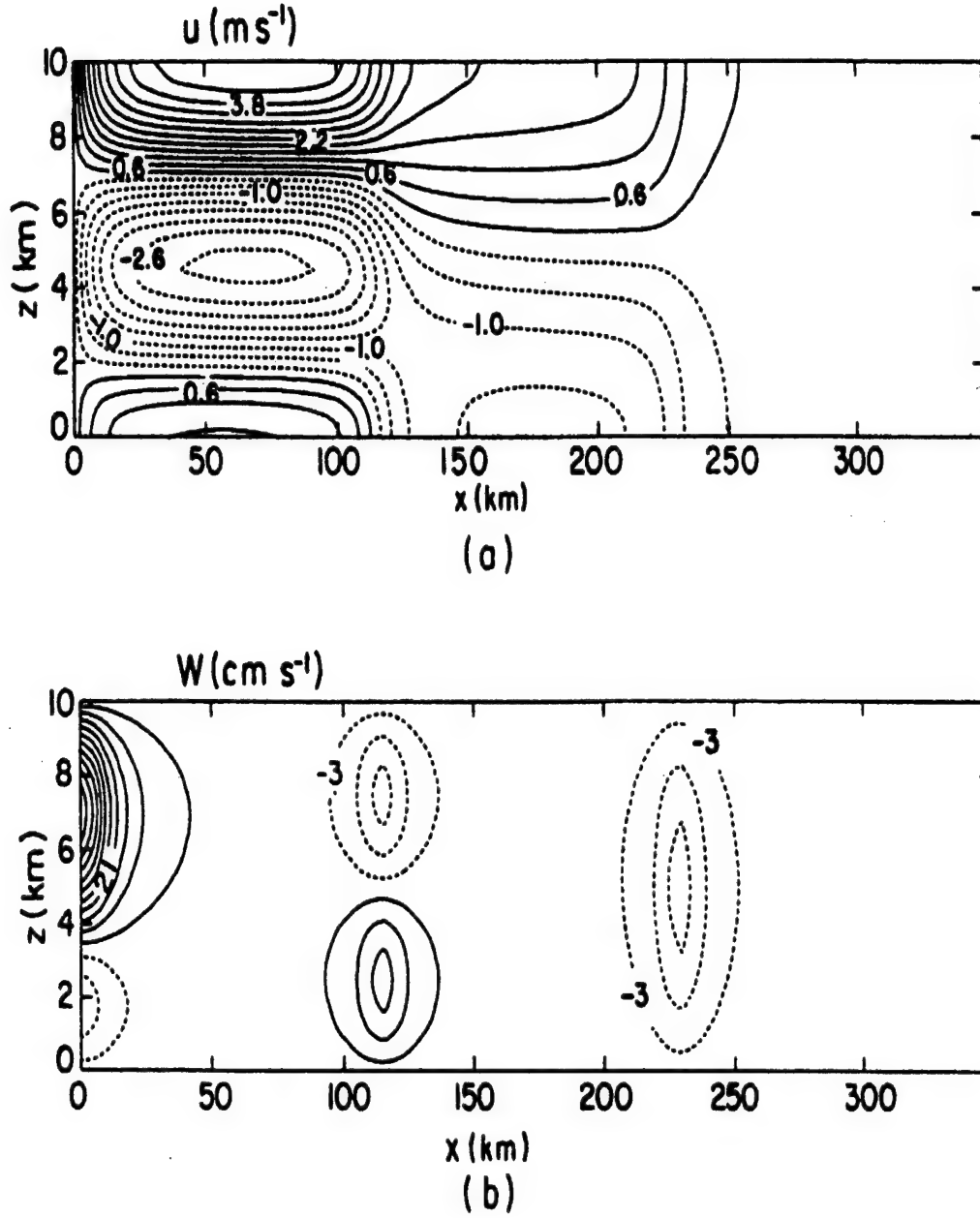


Fig. 5. Rigid-lid solution for the $n=1$ and 2 modes, adapted from Nicholls et al. (1991a), Fig 5. Vertical cross-section extending from thermal forcing at the left edge 2 hours after the initiation of the forcing. (a) Horizontal velocity tangent to the cross-section, normal to heat source. (b) Vertical velocity.

levels and is capped by a subsidence layer aloft. The resulting mid-level convergence produces strong mid-level flow toward the heat source with flow returning from the source to the mode-2 bore at both the surface and aloft (Fig. 5b). Mapes (1993) shows that similar results are obtainable by using a thermal forcing profile devoid of low-level cooling (Fig. 6). His profile also generates mode-1 and mode-2 bores, exhibiting the same behavioral characteristics as those that Nicholls et al. generate.

1.4. Motivation and Objectives

The goal of this paper is to investigate buoyancy bore behavior in a mesoscale model simulation using initial and boundary conditions from an actual convective outbreak in the central plains of the U.S. During this event a pair of MCSs moved to within approximately 60 km of each other, separated by an area devoid of convection. Despite low-level forcing produced by colliding outflow boundaries, convection failed to initiate between the two systems due to mid- to upper-level subsidence (Stensrud and Maddox 1988). The cause of this subsidence warrants further investigation. It is assumed that buoyancy-bore induced subsidence can be strong enough to maintain a low-level capping inversion in spite of strong low-level forcing for upward motion. Through an analysis of the behavioral characteristics of the buoyancy bores, it is hoped that their likely role in the suppression of new storm development between MCSs can be determined.

Chapter 2 of this paper describes the mesoscale model used and discusses the rationale for the initial and boundary conditions chosen as input for the simulations. This is followed by a detailed description of the procedures used to simulate a variety

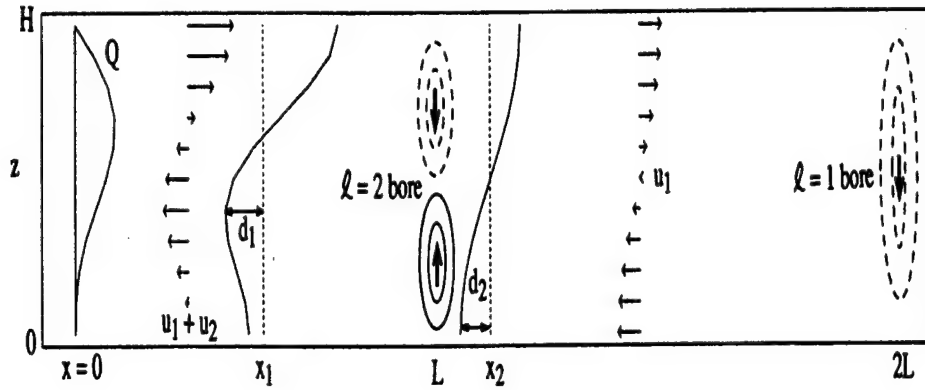


Fig. 6. Schematic of the buoyancy bores, horizontal winds, and integrated displacements of material lines (solid) relative to their initial positions (vertical dashed lines) a time τ after the initiation of the slab-symmetric heat source $Q(z)$ near $x=0$. The two buoyancy bores have reached L and $2L$, where $L=NH\tau/2\pi$. Note that the material lines have moved closer together at low levels, indicating area contraction remote from the heated region. Adapted from Fig. 5 of NPC (from Mapes 1993).

of convective regions that vary in size, magnitude, and duration. An examination of the convective parameterization scheme's (CPS) ability to generate a thermal forcing representative of observed and theoretical profiles also is discussed. Chapter 3 provides a detailed description of the behavioral characteristics of the buoyancy bores simulated. In Chapter 4, discoveries concerning the buoyancy bore behavior are then applied to a dynamic convective pattern to ascertain the likely impact of bore-related subsidence on the environment separating neighboring MCSs.

CHAPTER 2 - METHODS AND PROCEDURES

2.1. Model Description

This study uses the nonhydrostatic version of the Fifth-Generation National Center for Atmospheric Research/Penn State Mesoscale Model (MM5), Version 2 (Dudhia 1993; Grell et al. 1994). All simulations in this study use 23 levels of the terrain following vertical coordinate system σ . The model uses up to three two-way interactive nested grids, as shown in Fig. 7. This provides the ability to resolve mesoscale features without having to define the whole model domain at high resolution. The outermost coarse grid domain (grid 1) has 60 x 60 x 23 grid points with a horizontal grid spacing of 75 km. Within this grid is a nested grid domain centered on the central plains of the United States (grid2) with 61 x 61 x 23 grid points and a horizontal grid spacing of 25 km. The grid spacing of the innermost nested grid domain (grid 3) is 8.3 km and has 70 x 70 x 23 grid points.

Due to the coarse grid's inability to effectively resolve mesoscale features, all the simulations of convection are restricted to the two innermost grids. Furthermore, when examining convection on a particular grid, the convective parameterization is allowed to activate on that grid only, unless explicitly stated otherwise. This precaution is taken to minimize the influence of any grid-to-grid interactions on convection. Warner and Hsu (2000) show that the treatment of convection by the outer, coarser grids can greatly influence convection in the inner grids. By selectively changing the CPSs used in the outermost grid, they discover differences in the precipitation rates associated with the inner-grid, explicitly generated convection.

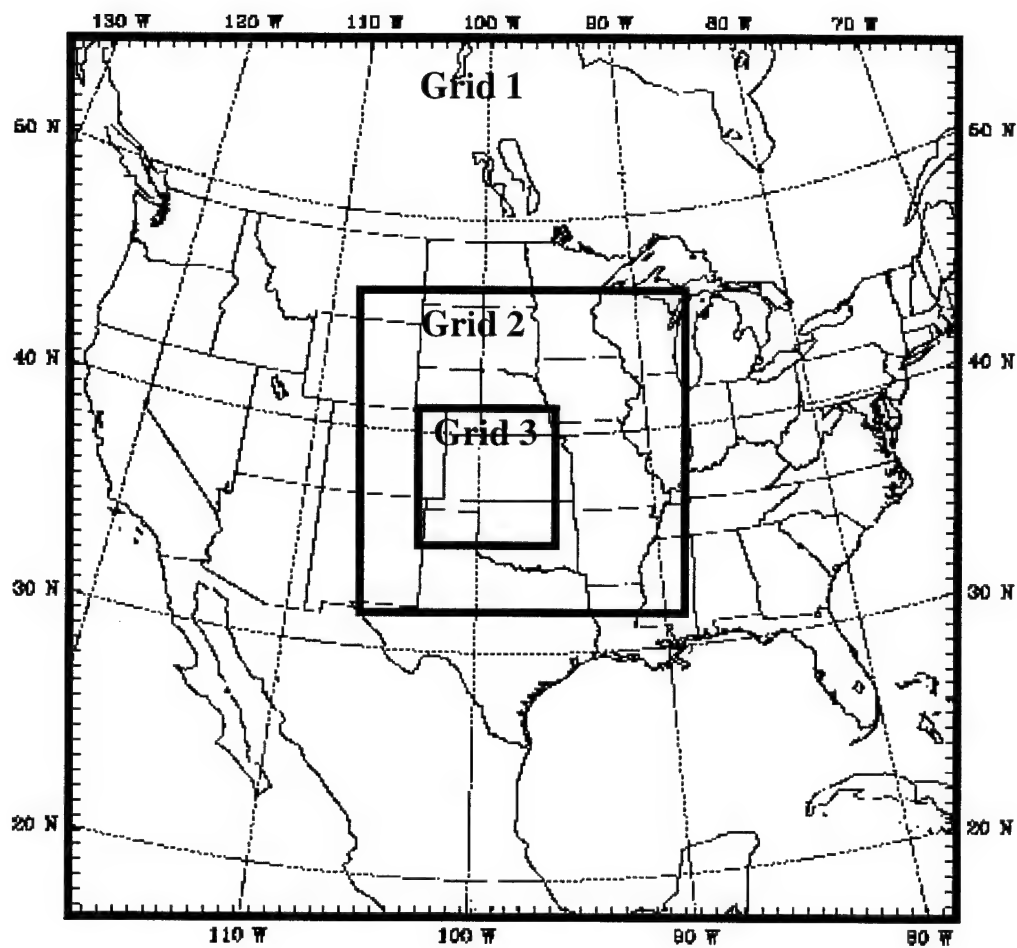


Fig. 7. A graphical representation of the grid locations used. The grid spacing for grids 1, 2, and 3 are 75, 25, and 8.3 km, respectively.

The differences in precipitation intensity, precipitation timing, and vertical distribution in latent heating associated with varying CPSs in the outer grid appear to influence the timing and intensity of convection on the inner grid through subsidence resulting from gravity-wave like features. This added subsidence, external to the grid of interest, could complicate our assessment of the vertical motions associated with the buoyancy bores of interest. By restricting the initiation of convection to a single grid, it is hopeful a more accurate appraisal of bore behavior is obtained. Also, due to the interactive nature of the nested grids, the innermost grid is disabled whenever convection is initiated on grid-2.

For ease of initiation, it is convenient to be able to simulate convective heating regions (CHRs) anywhere in the domain for any chosen time period. This can prove difficult. Naturally, the atmosphere is not conditionally unstable at all places and at all times within the grid domain. Although the initiation of convection can be forced in the CPS, sufficient low-level moisture must be present in order to generate a realistic vertical profile of thermal forcing.

One mechanism by which moisture is increased within the lower atmosphere is through latent heat fluxes from the ground surface. The MM5 parameterizes this process by utilizing the force-restore method (Deardorff 1977). A constant moisture availability value of 0.6 is used across the entire domain to allow for the development of a moist boundary layer.

The Burk-Thompson Planetary Boundary Layer (PBL) scheme (Burk and Thompson 1989) also is selected for use in the simulations. This scheme as used in the MM5 differs slightly from that described in Burk and Thompson (1989). It

neglects the countergradient terms in the fluxes of heat and moisture as well as the effects of liquid water (Braun and Tao 2000). This scheme results in less detrainment in the PBL. This feature, coupled with the constant moisture availability of 0.6, leads to realistic vertical heating profiles resulting from the convection in our simulations.

2.2. Selection of Initial and Boundary Conditions

The data used in this study are from a convective outbreak over the central plains on 23-24 June 1985. On this day, described in detail by Stensrud and Maddox (1988), several MCSs are observed and shown to interact. Within such an environment, it is possible to manually initiate realistic CHRs in a variety of sizes and patterns and explore the behaviors of the resulting buoyancy bores. The model is initialized using a first guess field from the NCEP global analysis at $2.5^\circ \times 2.5^\circ$ resolution and surface and rawinsonde data are blended-in following the technique of Benjamin and Seaman (1985). The model is started at 1200 UTC 23 June 1985.

2.3. Simulation Procedures

A series of model simulations are performed starting from this initial time. The first simulations are non-convective runs. Within these runs, the CPS is disabled on each of the three grids. For file size continuity, non-convective runs of different durations are necessary in order to correspond with the varying durations of the different convective simulations. The purpose of the non-convective run is to establish a base-state atmosphere, without convection. A series of convective runs follow, each with different spatial and temporal characteristics of convection. These

runs are created by employing a technique of temporal and spatial initiation/suppression of convection within the Kain-Fritsch CPS. Thus, individual CHRs are created, varying in size from roughly 69 to 10^4 km^2 , and placed in different areas within the grids. A total of 34 different runs are created and examined. For simplicity, those runs actually presented in this paper all have the same CHR dimensions and locations in space, regardless of the grid in which they are placed (Fig. 8). This allows for more accurate inter-grid comparisons.

Typically, the specified CHR encloses 5625 km^2 , corresponding to a square of 75 x 75 km. On grid-2, this equates to a 4 x 4 grid-point box, since each grid-point is separated by 25 km. Given the $3:1$ ratio of grid-2 grid spacing to grid-3 grid spacing, an equivalent grid-3 CHR has the dimensions of 10 x 10 grid-points. The grid points activated in these convective heating regions are indicated in Table 1a. In addition to the production of individual convective regions, convective region pairings are created. The pairings are formed by creating an additional CHR south of the original (Fig. 8b). The distance between these regions varies from 50 to 300 km, but those shown in this paper are generally separated by 75 km (Table 1b). Examinations of these pairings are performed in order to ascertain the effects that interacting buoyancy bores have on the environment separating neighboring convective zones.

The initiation of the CHRs in this paper occurs at six hours after the start of the model run, and the simulations continue for an additional 6 hours. After that point, any bores produced dissipate to a point where they can no longer be adequately resolved (Lin and Goff, 1988).

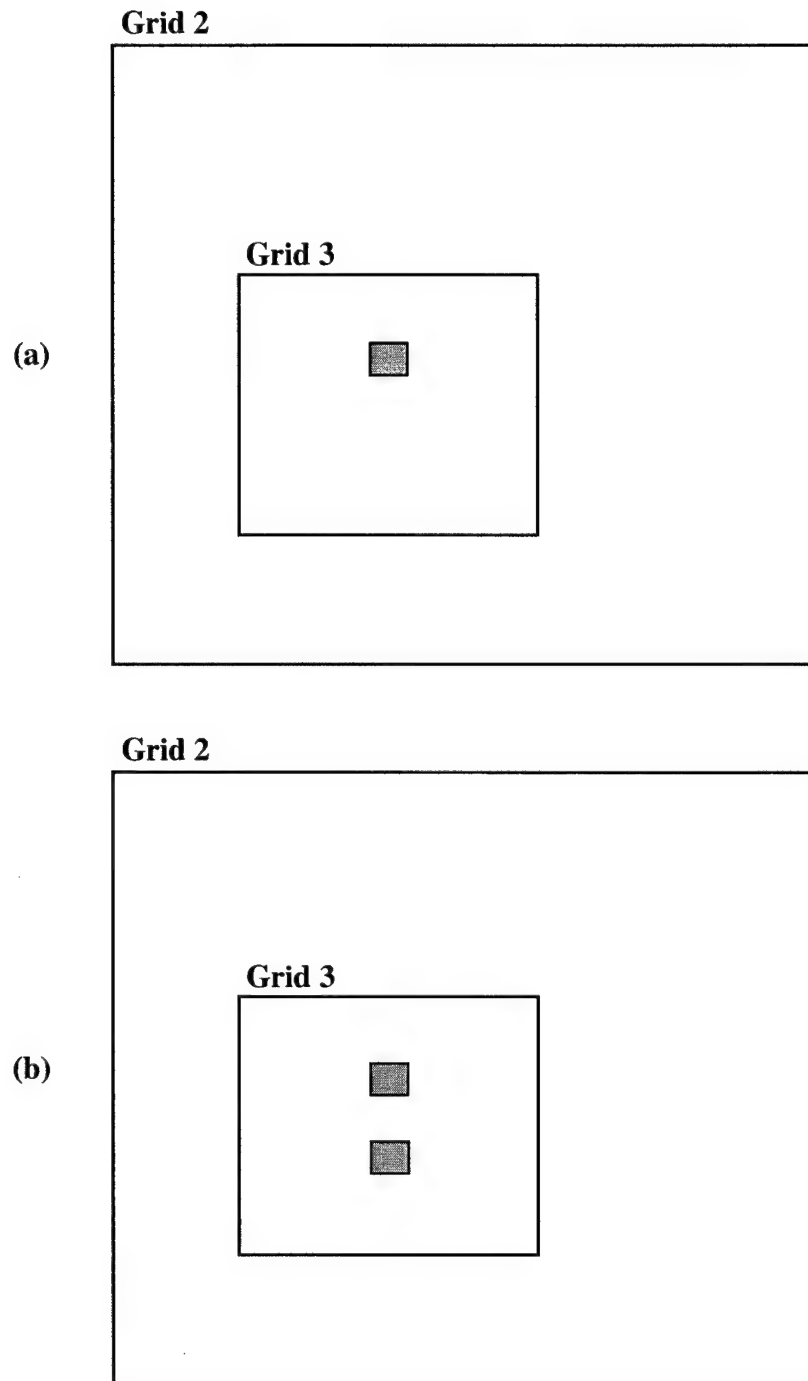


Fig. 8. Approximate size and placement of convective heating regions (shaded areas) within both grid 1 and 2. (a) Solitary region. (b) Convective region pairings.

	Corners of Convective Heating Regions (x , y)			
	NE	SE	SW	NW
Grid-2	(24 , 31)	(24 , 28)	(21 , 28)	(21 , 31)
Grid-3	(39 , 49)	(39 , 40)	(30 , 40)	(30 , 49)

(a)

	Corners of Convective Heating Regions (x , y)			
	NE	SE	SW	NW
Grid-2	(24 , 28)	(24 , 25)	(21 , 25)	(21 , 28)
Grid-3	(39 , 40)	(39 , 31)	(30 , 31)	(30 , 40)

(B)

Table 1. Coordinates of the outer corners of the (a) primary convective heating region used for analysis and (b) the additional convective heating region used to create a pair of convective heating regions.

While exploring a variety of convective scenarios, the duration of thermal forcing may differ from one CHR to another. For the cases described in this paper, unless otherwise stated, the applied thermal forcing to the CHR is continuous.

Output from both the convective and non-convective simulations is fed into a program specifically designed to process MM5 output data. The specific parameters of interest (such as the u, v, and w components of the wind, temperature, pressure, and specific humidity) are coupled with a pressure related term in MM5. These variables first are decoupled to effectively isolate the true value of the variables. Then the output parameters from the non-convective run are subtracted from those of the convective run and re-coupled with their pressure related terms to yield a MM5 output file consisting of the perturbations resulting from convection alone. This provides a much cleaner picture of the atmospheric disturbances resulting solely from convection. By examining these perturbations, the behavioral characteristics of buoyancy bores are more easily ascertained.

2.4. Thermal Forcing Profile

To fully understand the behavioral characteristics of buoyancy bores generated by the CHRs in this study, it is important to ascertain both the convective heating profiles and the total temperature tendencies as a function of space and time for the grid points at which convection is active. The vertical heating profiles are extracted directly from the K-F scheme at the grid points where convection is initiated. A composite of the typical thermal forcing that is seen (Fig. 3b) shows that the upper-level thermal forcing is in good agreement with that of Figs. 3a and 3c. One of the

more notable differences is the shallowness of the low-level cooling. As mentioned earlier, Mapes (1993) shows that the production of mode-1 and mode-2 bores is not dependent upon the low-level cold forcing; the dominant factor is the placement of maximum forcing in the upper troposphere.

Another interesting feature seen in Fig. 3b is the atmospheric heating found near 900 hPa. An interrogation of environmental soundings from that day seems to explain this feature. Although there is a sufficient moist layer near the surface, a low-level capping inversion is evident over much of the model domain at or near 900 hPa. Obviously, this layer is devoid of convective available potential energy (CAPE). Considering the dry nature of this stable layer, any ascent due to convection would result in a comparatively lower mass flux at that level due to detrainment. Above this layer, the conditionally unstable profile demonstrates a significant amount of CAPE. Such high CAPE profiles have been shown to be associated with much larger mass flux values than drier, low CAPE profiles (Kain and Fritsch 1990). A comparison of parameterized convective heating profiles (Fig. 9) shows the scheme's sensitivity to environmental relative humidity. The dry, low-CAPE profile (Fig. 9a) shows a peak in environmental heating near 900 hPa. Whereas, the convective heating profile of the high-CAPE case has the bulk of its heat released near 400 hPa (Fig. 9b). Using the near-900 hPa values of Fig. 9a to represent the dry capping inversion found in our model environment, and superimposing them onto the lower portion of the high-CAPE profile of Fig. 9b, we can envision a profile very similar to that generated by the K-F scheme shown in Fig. 3b.

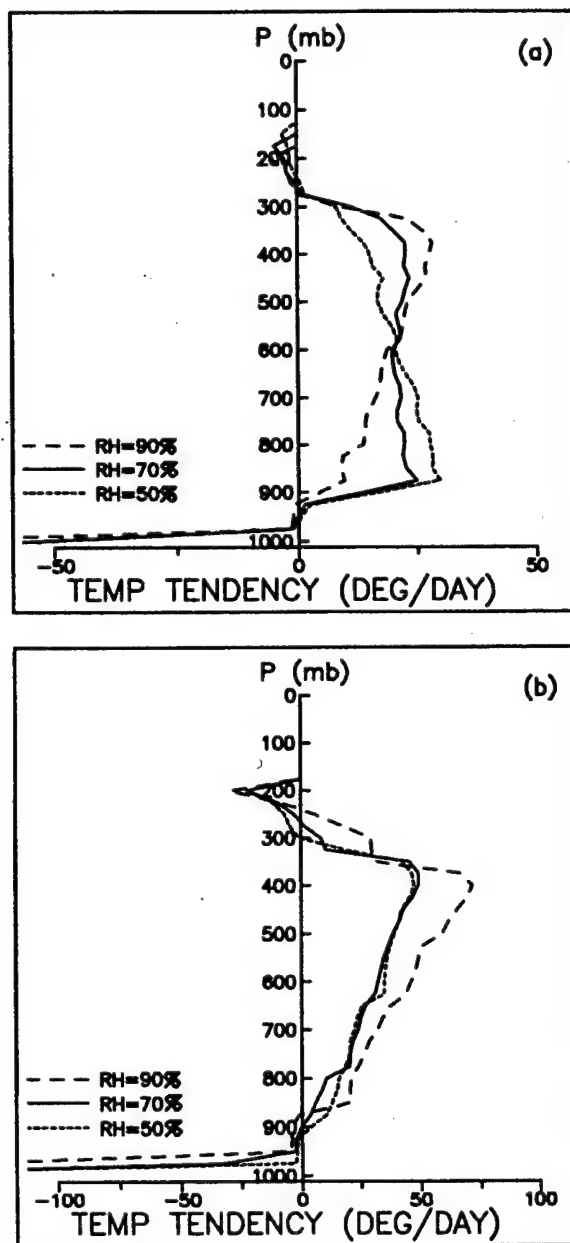


Fig. 9. Parameterized convective heating profiles corresponding to a (a) dry, low-CAPE environment and (b) a moist, high-CAPE environment (from Kain and Fritsch 1990).

With a reasonable thermal forcing profile established by the K-F scheme, the total temperature tendency is written out at every model time-step at grid points with forced convection in order to determine the response of the model to the heating profile prescribed by the K-F scheme.

CHAPTER 3 - MODEL-GENERATED BUOYANCY BORES

3.1. Identification/Recognition of Buoyancy Bores

Analysis of the atmospheric lapse rate, depth of the troposphere, and upper-tropospheric temperature are necessary to determine the typical propagation speed of a bore, as calculated in (3). In addition to these factors, the environmental wind field also is examined, since it has been shown that the propagation of bores is influenced by the mid- and upper-tropospheric flow (Lin and Goff 1988). Bores moving with the flow travel faster than those propagating against it. By examining the area surrounding a given CHR, an estimation of the propagation speed of a bore emanating from this heat source is made. Once detected, features demonstrating this behavior are interrogated further to ascertain whether or not they are buoyancy bores. This is done by examining the horizontal and vertical wind fields to determine if the wind field response is consistent with theory.

Due to its large vertical extent and rapid translation speed, the most prominent and identifiable mode of buoyancy bores is mode-1 bore (Fig. 10). It manifests itself as an area of concentrated, negative vertical motions that propagates away from the convective region. Notice the vertical orientation of the bore at just 6 minutes ($t + 6$ min) after convective initiation (Fig. 10b). This orientation is very similar to that in the Nicholls et al. (1991a) simulation (Fig. 5). However, an important difference between the bores generated here and those from the idealized simulations is the vertical placement of the bore vertical velocities. The rigid-lid simulations depict vertical motions in the bores as being symmetric in the vertical, centered midway

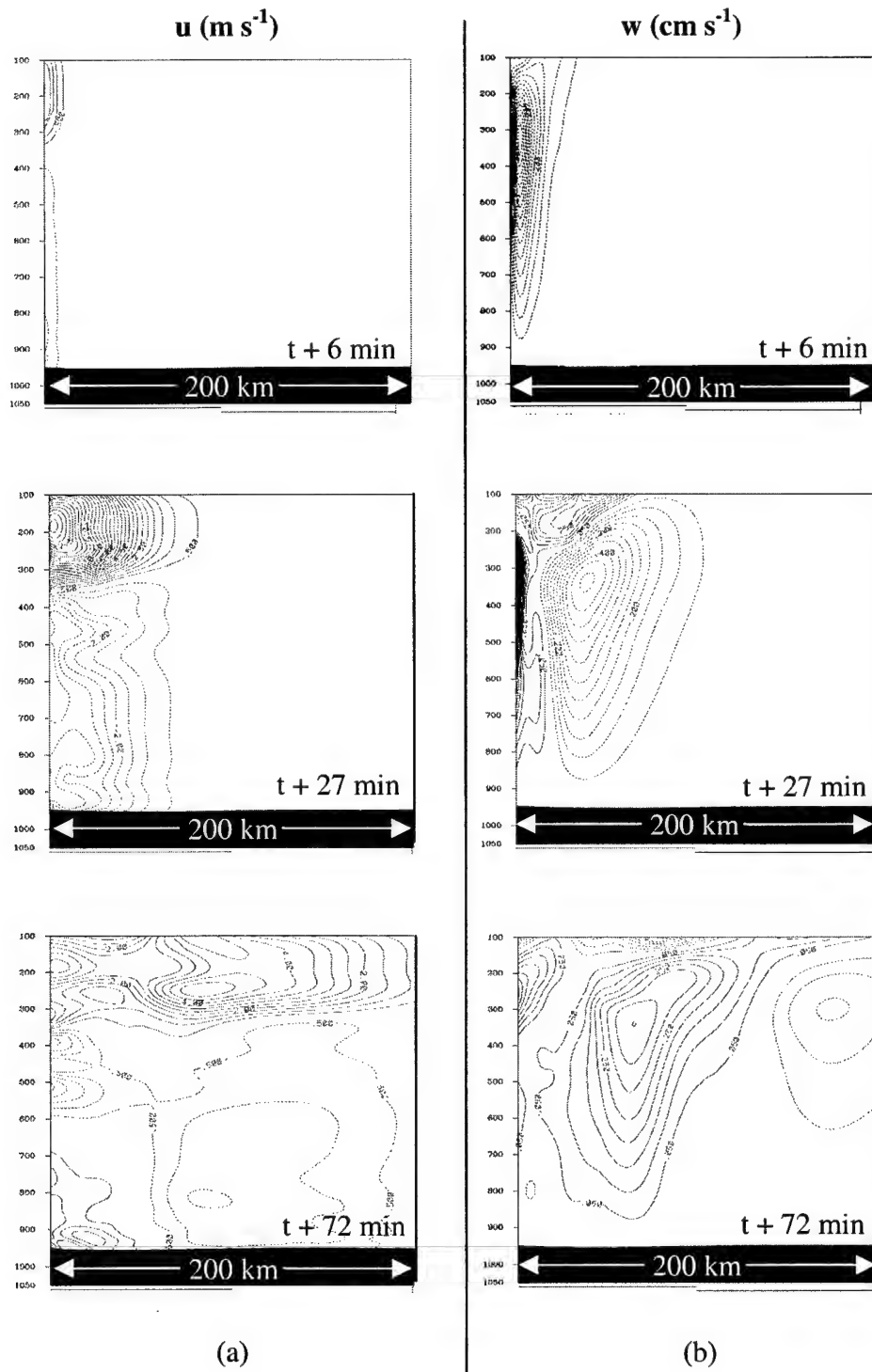


Fig. 10. Vertical cross-section extending from thermal forcing at the left edge. The vertical scale is measured in hPa. (a) Horizontal velocity tangent to the cross-section, normal to heat source. The contour interval is 0.5 m s^{-1} . (b) Vertical velocity, contour interval is 5 cm s^{-1} .

between bottom and top of the domain (Nicholls et al. 1991; Mapes 1993). In this study, vertical motions in the mode-1 buoyancy bores are maximized about the level of maximum thermal forcing which, owing to the environmental thermodynamic profile, is always in the upper troposphere (generally between 300 and 350 hPa). Generating bores nearer to the tropopause than the surface yields a shallower outflow aloft from the heat source to the bore, and a deeper return flow from the bore below the level of maximum thermal forcing (Fig. 10a). Therefore, early in its lifecycle, horizontal wind flow owing to mode-1 buoyancy bores is almost entirely toward the convective cell over a majority of the troposphere. A similar behavior is seen in a two-dimensional Florida sea breeze simulation by Nicholls et al. (1991b).

To verify that the correlation between the level of max heating and the level of the maximum vertical motions of the bore is not coincidental, the convective thermal forcing profile produced by the K-F scheme is forced to resemble a vertical half-sine wave (Fig. 4a). This artificial thermal forcing profile produces a maximum heating near 480 hPa. The subsidence resulting from a mode-1 buoyancy bore shortly after the initiation of the thermal forcing indicates that the bore is centered about the 480 hPa level -- the level of maximum heating (Fig. 11a). A similar response is seen between a thermal forcing maximum near 700 hPa and the resulting bore (Fig. 11b). Although not exact, the correlation of the bore to the level of maximum thermal forcing is unmistakable.

Results also show that the vertical structure of the bores (Fig. 10b) skews with time. Notice that initially the bore is almost vertically stacked (Fig. 10b). As it

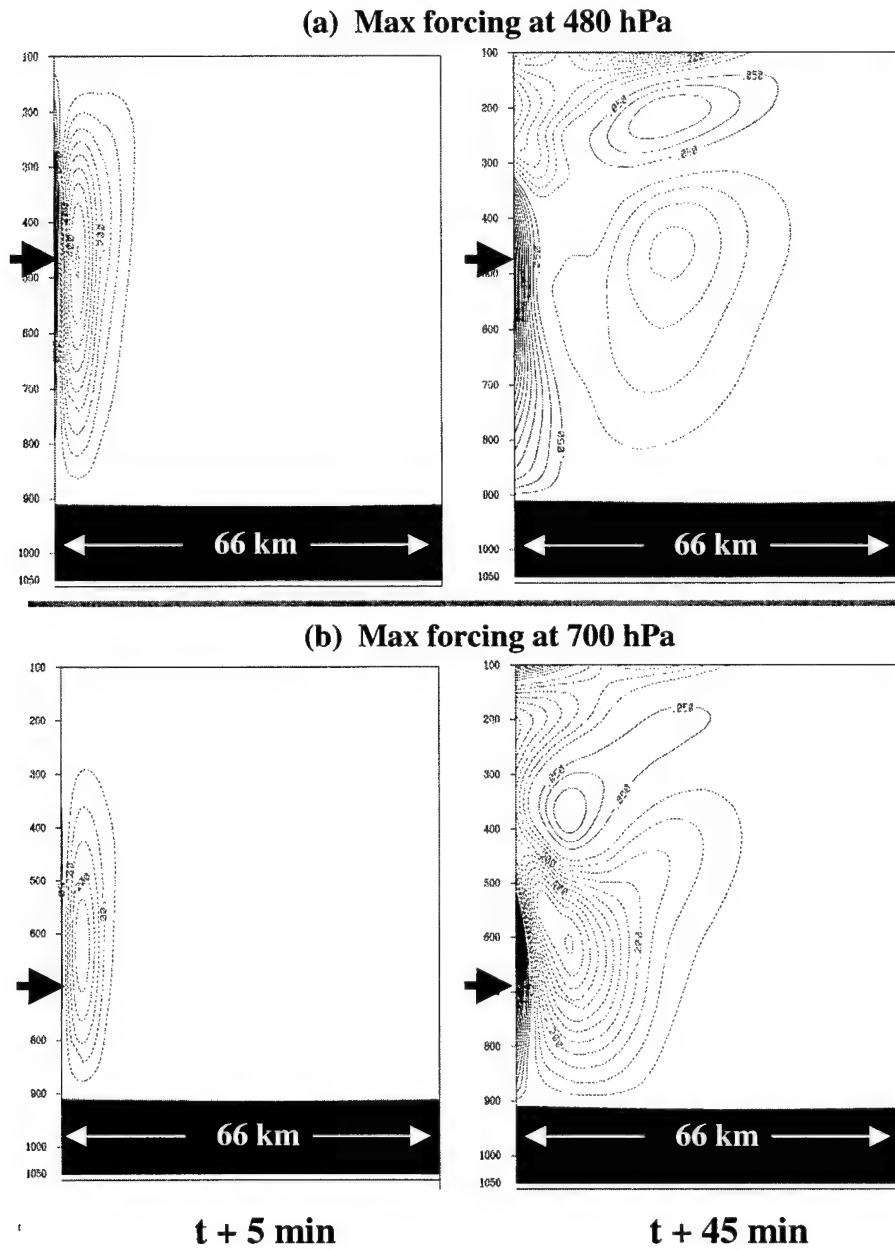


Fig. 11. Vertical velocity cross-sections; contour interval as in Fig. 10. A thermal forcing profile is applied to the left edge with a maximum near (a) 480 hPa, and (c) 700 hPa.

progresses in time and space, the portion of the bore extending into the stratosphere propagates at a greater speed than the portion of the bore residing in the troposphere. This behavior is consistent with (3) which shows that the propagation speed of the bore is proportional to the Brunt-Väisälä frequency

$$N = \left[\frac{g}{\theta} \frac{\partial \theta}{\partial z} \right]^{1/2}, \quad (4)$$

where θ is the potential temperature, g is the acceleration due to gravity, and z is the height in the atmosphere. Thus, the increased stability of the stratosphere leads to greater values of N at this level, as shown in Fig. 12. This in turn leads to faster bore propagation. This behavior is evident in the numerical simulations of Pandya et al. (1993). Also, recall that the environmental wind flow can affect the propagation speed of a bore. Therefore, vertical wind shear also plays a role, albeit small, in the deformation of a bore.

By examining the evolution of these bores, it is seen that the intensity of the bore steadily decreases as it propagates. This behavior also is observed by Bretherton and Smolarkiewicz (1989). It is partly attributed to the lateral spread of the wave as it propagates outward in all directions from the source region and partly to energy loss into the stratosphere (Lin and Goff 1988).

3.2. *Thermal Forcing Dependence*

Results indicate that the catalyst for buoyancy bores is thermal forcing. So, as might be expected, many of the properties of a bore are a function of the thermal forcing applied. Various sensitivity tests indicate that although the thermal forcing

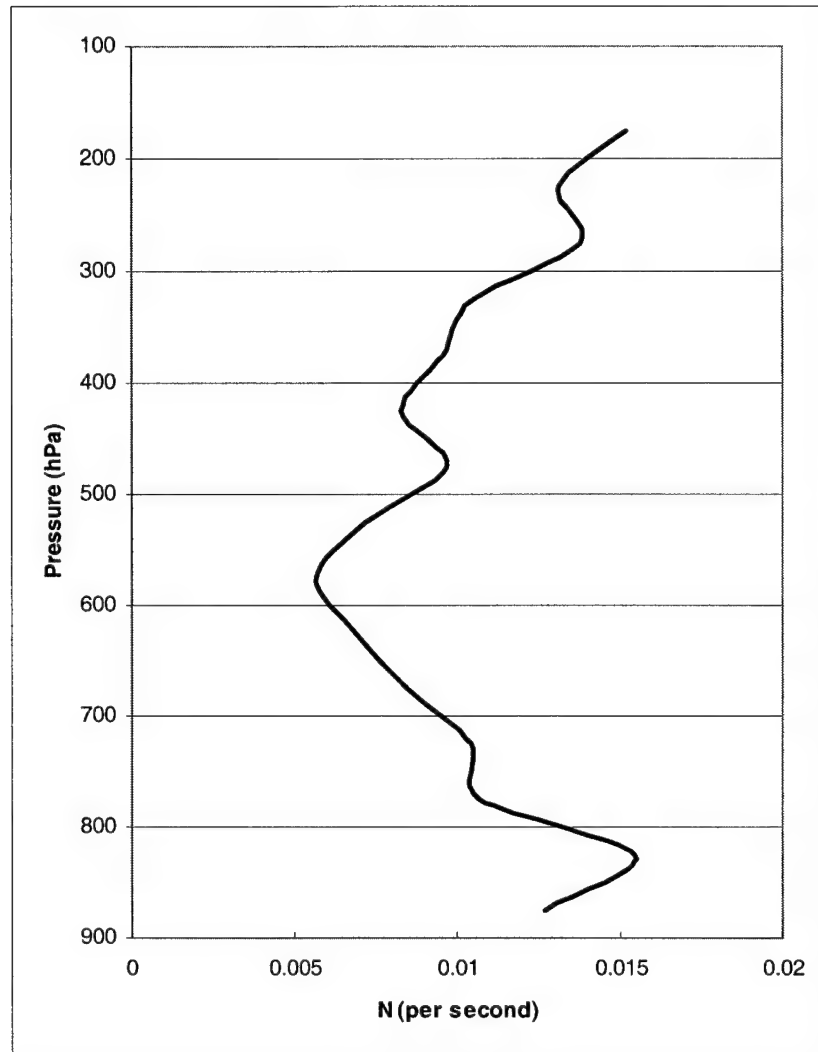


Fig. 12. Vertical variation of the Brunt-Väisälä frequency (N) obtained from an atmospheric profile typical of those extracted from the model simulations found in this paper.

profile may have multiple levels where heating is applied, the maximum vertical motion associated with the bore is found at the level of the maximum heating.

As expected, results also suggest that the magnitude of thermal forcing has a direct influence on the intensity of the resulting bore. A comparison of two bores produced by the identically shaped heating profile, but with different magnitudes of forcing (Fig. 13a,b) shows that the stronger the thermal forcing the stronger the buoyancy bore (Bretherton and Smolarkiewicz 1989; Nicholls et al. 1991a).

The duration of the applied thermal forcing also affects the intensity of the bore. A comparison of simulations using a continuously applied thermal forcing with simulations using a thermal forcing of only a few minutes duration shows that, initially, the bores are identical (Fig. 14). However, once thermal forcing is discontinued, the decay rate for the bore is greater without the continual thermal heating in the source region than the decay rate in an environment of continuous thermal forcing. More persistent thermal forcing results in a longer-lived, more intense bore. This also is consistent with theory which shows that bore intensity is related to the total heating applied (Nicholls et al. 1991a).

Lastly, the horizontal extent of the CHR also affects the intensity of buoyancy bores. Given an equivalent thermal forcing at every grid point within a CHR, the larger the region, the greater the mode-1 bore subsidence, as expected (Bretherton and Smolarkiewicz 1989). The comparison of the simulated buoyancy bores with theory shows that the behaviors of the bores are consistent with expectations. We now turn to a more interesting investigation of bore interaction.

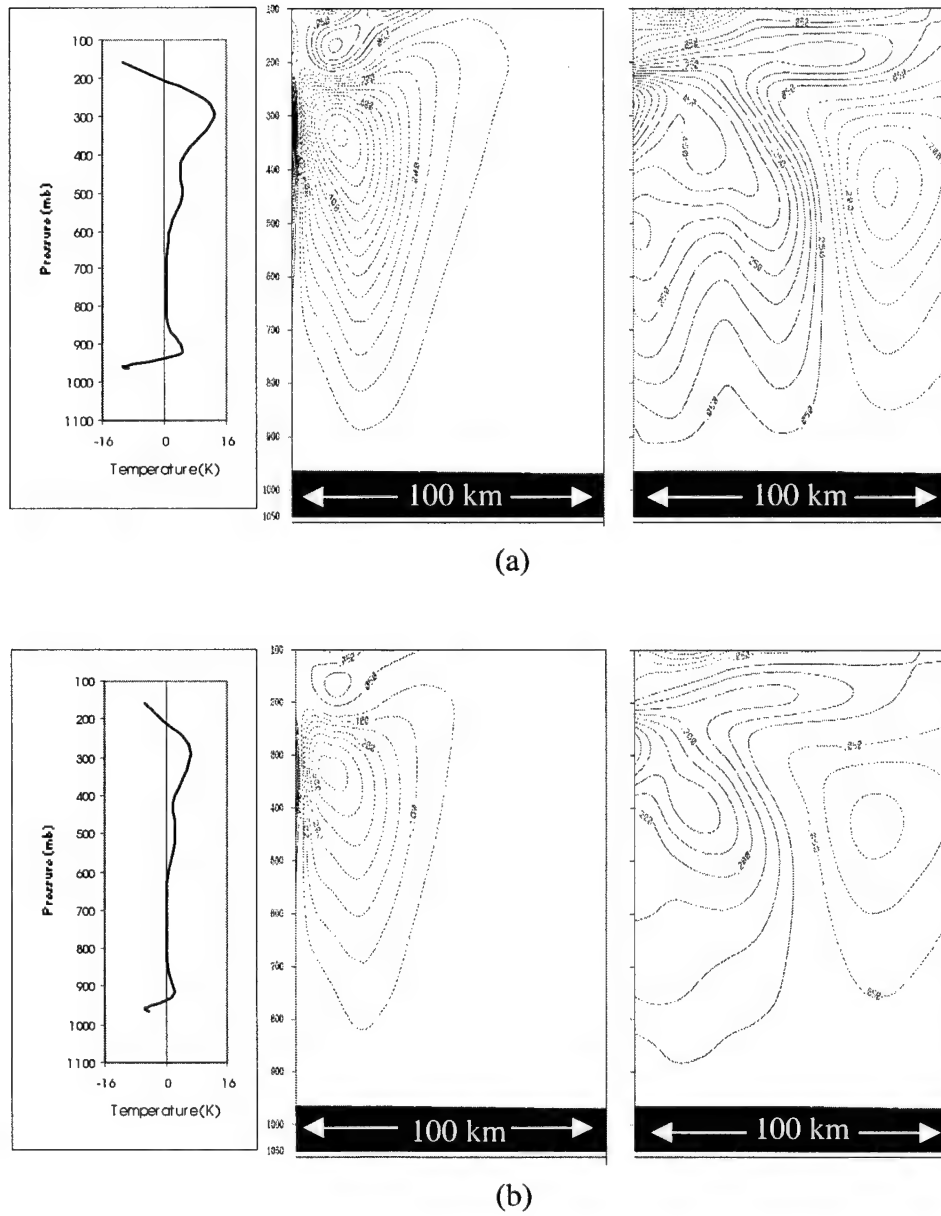


Fig. 13. Sensitivity of model solution to different thermal forcing profiles. Thermal forcing profiles are shown to the left. (a) Vertical velocity response to standard thermal forcing. (b) Vertical velocity response to a thermal profile differing only in magnitude from (a). Contour intervals are as shown in Fig. 10.

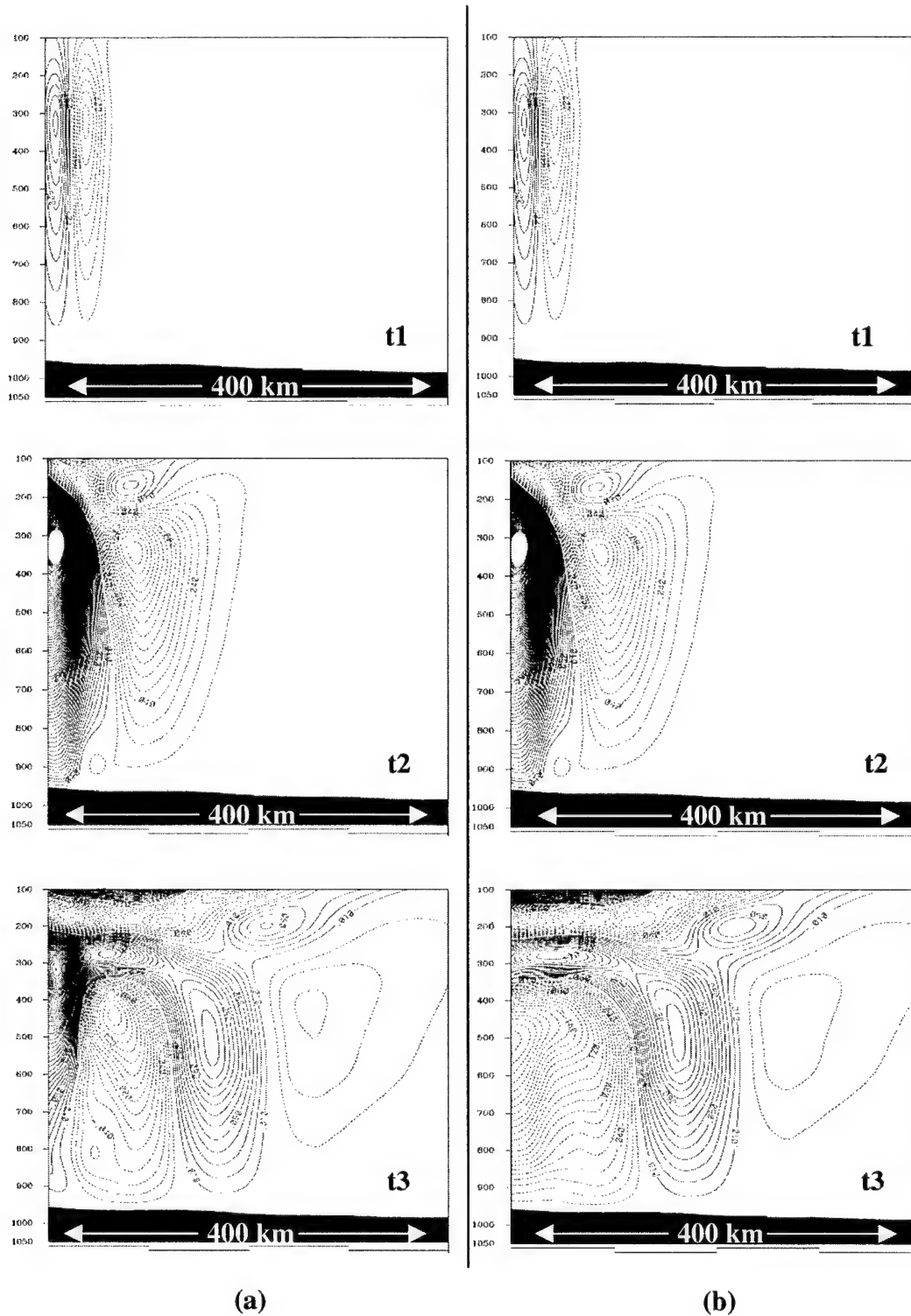


Fig. 14. Vertical cross-section of vertical velocity extending from thermal forcing at the left edge. The vertical scale is measured in hPa. The contour interval is 5 cm s⁻¹. (a) Persistent heat source. (b) Heat source removed after 45 minutes (t2).

3.3. Bore Interactions Between Thermal Forcing Regions

In addition to the behavior of individual buoyancy bores emitted from a single CHR, it is important to understand the behavior of bores in the area between a pair of CHRs. More specifically, how do bores from neighboring convective regions interact in the area separating the two regions? With two CHRs in close proximity, initiating at nearly the same time, emitting buoyancy bores radially in all directions, it is inevitable that in a cross-section connecting the two there would be two bores approaching each other and interacting. An understanding of this interaction may help us gain a better understanding of the role bores play in the suppression, or enhancement, of convection between neighboring MCSs.

In Fig. 15 it can be seen that as two bores approach one another their mere proximity appears to result in an increased subsidence. Due to the skewing effect described earlier, the bores first interact in the stratosphere with the overall subsidence at that level equivalent to the cumulative subsidence of the individual bores at that space and time. As they continue to approach each other, their additive effect creates a wider, more intense subsidence region with the maximum still concentrated in the upper troposphere. As might be expected, the subsidence resulting from the bore interaction reaches its maximum when the two bores overlap each other, occupying roughly the same space (Fig. 16). As the bores continue to pass through each other, they regain their individual characteristics, seemingly unchanged by their interaction with each other.

The size and intensity of the cumulative bore is in part a function of the distance between the two CHRs. The further apart the regions are the longer it takes for the

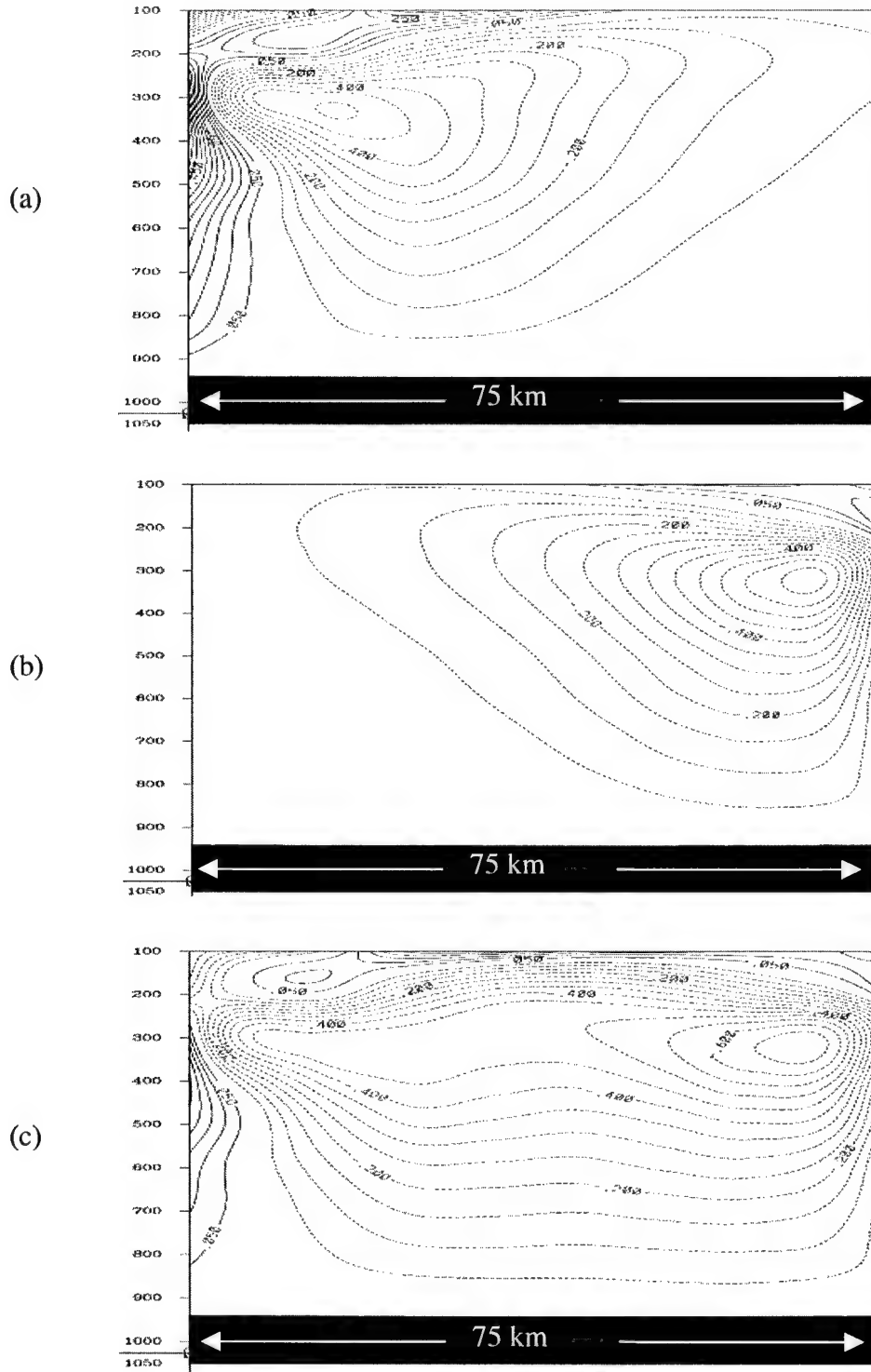


Fig. 15. Buoyancy bore(s) related vertical velocities at 10 minutes after convective initiation. Units as in Fig. 14. Thermal forcing at (a) the left boundary only, (b) the right boundary only, and (c) at both boundaries.

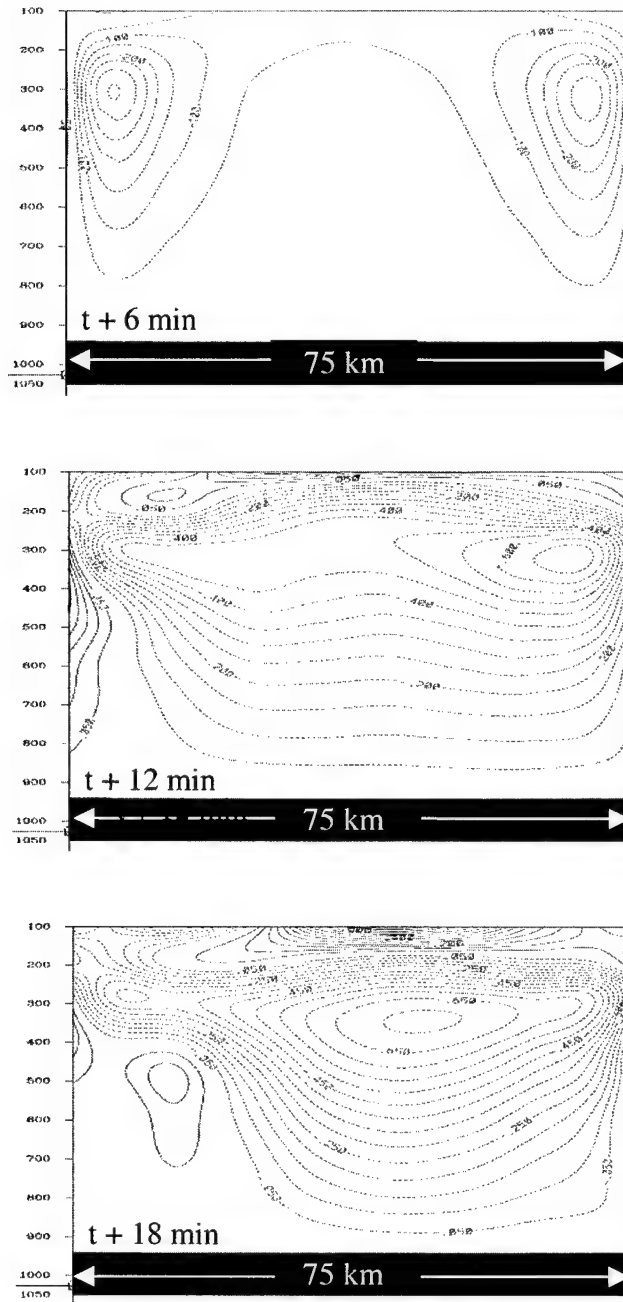
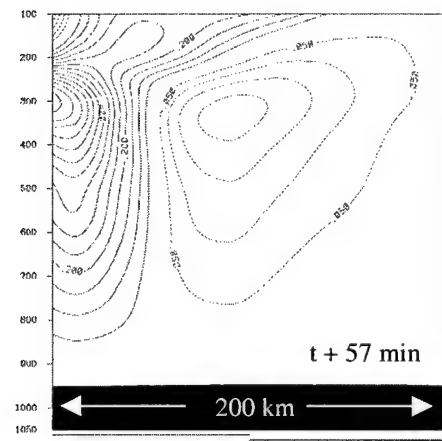
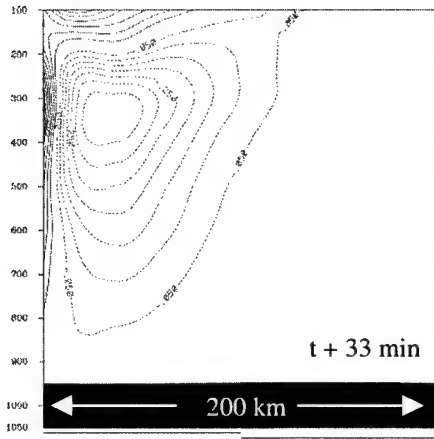
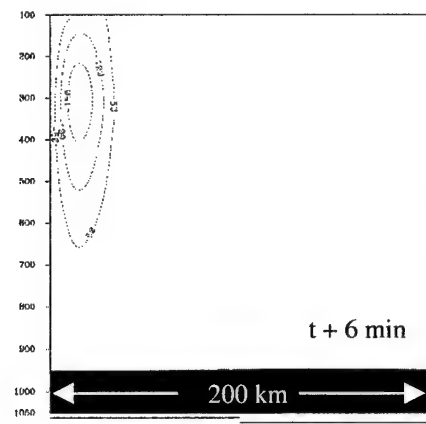


Fig. 16. Time series of vertical velocities taken between two areas of thermal forcing. Forcing applied at both the left and right edges of cross-section. Bores overlap each other at $t + 18 \text{ min}$. Contour interval and vertical coordinate are the same as in Fig. 14.

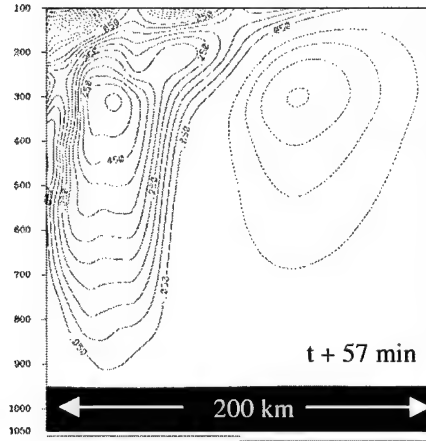
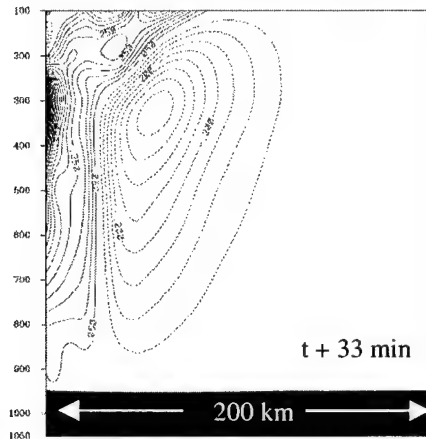
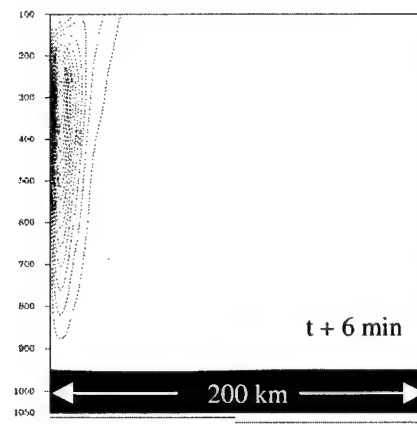
bores to reach each other and, due to the dissipative nature of bores, the weaker the bores are once they finally come into proximity of each other. Due to the skewing properties of bores, this time delay also allows the bores to become more vertically skewed. This results in a broader cumulative bore. In other words, the closer the two CHRs are to each other at initiation, the more intense, narrow, and short-lived is the cumulative subsidence. At greater separation, broader, longer lasting, yet weaker cumulative subsidence regions result from the bore-to-bore interaction.

3.4. Grid Scale Dependence

The aforementioned bore characteristics are observed on each of the two innermost grids of 25 and 8.3 km. Separately, there seems to be very little difference in bore behavior between the coarser grid and the finer mesh grid, but a closer examination reveals subtle differences. By comparing two independent simulations, each initiating an identical region of convective heating, the contrast in mode-1 buoyancy bore behavior becomes evident. In each grid, the CHR is located in the same place, and initiated at the same time. The thermal forcing profiles from the K-F scheme are identical and constantly applied. Examination of the pre-convective environment shows no appreciable difference between the two simulations. Once the thermal forcing is applied, the differences are noticeable (Fig. 17). At the onset of thermal forcing, the subsidence from the finer-scale grid bore is much more intense than that from the coarser grid. This result is not surprising since the inability of grid-2 to produce a bore with the same intensity as grid-3 is due to the coarser grid's inability to fully resolve this small-scale feature. Grid-3, with its finer grid spacing,



(a)



(b)

Fig. 17. Time series of vertical velocity in response to thermal forcing. The contour interval and vertical scale are as in Fig. 14. The thermal forcing is applied to the left edge of the cross-sections. Both (a) and (b) are subjected to the same thermal forcing at the same points in time and space. (a) Solution using a grid spacing of 25 km. (b) Solution using a grid spacing of 8.3 km.

can better resolve the bore and therefore more closely portray its intensity. However, buoyancy bores also demonstrate a slightly greater propagation speed and dissipation rate on the finer grid than the coarse-grid. This is likely due to differences in the treatment of diffusion on the two grids (see Xu et al. 2001). In general, buoyancy bores generated on either grid tend to have roughly the same intensity by about 1 hr after convective initiation; they are both rather weak. Thereafter, the magnitudes are so small that differences between the two are indiscernible.

3.5. *The "Inverse-bore"*

In the course of this study, an unanticipated yet persistent feature is revealed. This feature is quite evident in Fig. 14, given the large horizontal extent of this cross-section. Just behind the mode-1 buoyancy bore, nearer the source of thermal forcing, is a near mirror image of the bore. Although they have similar dimensions, the feature produces vertical motions of opposite sign to the bore - ascent rather than subsidence. Given this property of the feature, and for ease of reference, it is referred to as an "inverse-bore". At first glance, it appears that the inverse-bore is more intense than the bore it is associated with, but closer examination shows that this is not the case. The inverse-bore is generated some time after the initial bore, yet within the time period for which the K-F scheme heating profile is applied. Its rate of propagation is usually equal to or less than that of the initial bore, and its dissipation rate is quite similar. Therefore, the comparison of the intensity of the two should not be made at the same point in time, but instead, at the same point in space. If you compare the magnitude of the bore at a given space and time with that of the inverse-

bore at the same place at a later time, then they are of similar magnitude. Therefore, a parcel experiencing descent due to the passage of a buoyancy bore will later experience a similar amount of ascent due to the associated inverse-bore. In fact, because the inverse-bore quite often propagates at speeds less than the initial bore, a parcel can be under the influence of an inverse-bore for a greater amount of time than it was for the initial mode-1 bore. Thus, the net effect can often be an overall ascent once the two features have passed. This discovery is significant in the quest to ascertain the role buoyancy bores play on the suppression of convection. Therefore, this poses an important question: What causes these inverse-bores to occur while convection is still active?

A clue to this question is revealed by Nicholls et al. (1991a). They show a feature that manifests itself once the thermal forcing is removed (Fig. 18b). This feature is very similar in appearance and behavior to the inverse-bores observed in this study. But there is a significant difference. Our inverse-bores are evident regardless of the duration of thermal forcing; even in simulations of continuous thermal forcing from the K-F scheme, inverse-bores develop.

This contradiction is resolved by examining the differences between the simplified model used by Nicholls et al. and the MM5 used in this study. Specifically, Nicholls' model provides no atmospheric feedback to the applied thermal forcing, whereas the MM5 does. The vertical profile of thermal forcing provided by the K-F scheme introduces a local heat source within MM5 when initiated. Initially, the atmospheric response somewhat mirrors the intent of the K-F

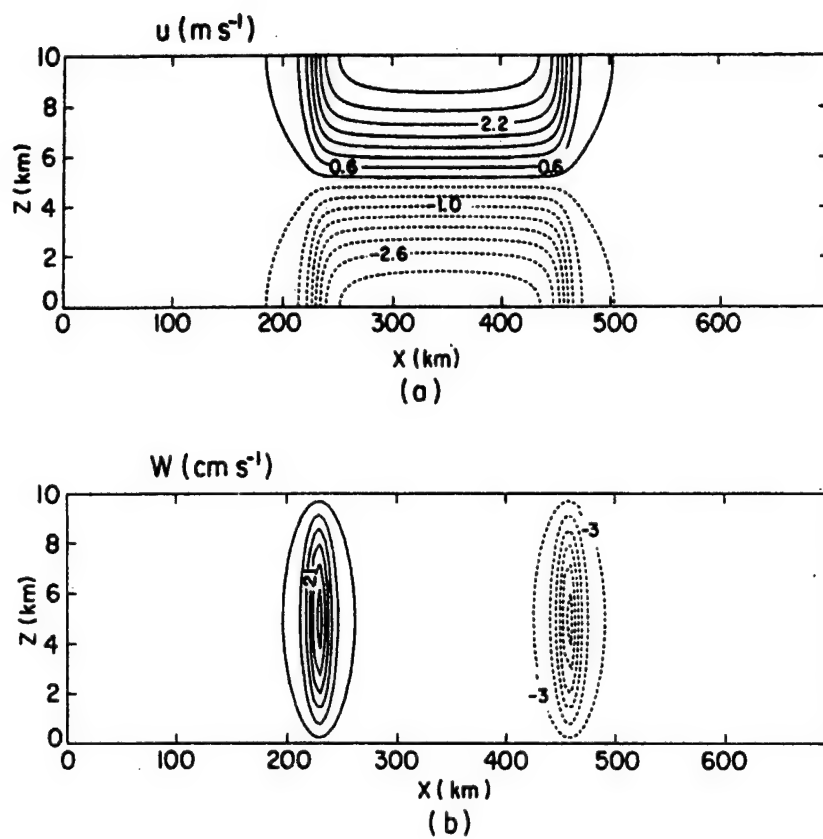


Fig. 18. Solution for a pulse forcing with a duration of 2 hrs. Units same as in Fig. 5. Figures are from 2 hrs after the termination of forcing (adapted from Nicholls et al. 1991a)

scheme and a bore is produced (Fig. 19). As time progresses, vertical advection processes begin to offset the thermal forcing of the K-F scheme. Eventually, the cooling due to the ascent of buoyant air becomes greater than the heating due to the thermal forcing of the K-F scheme. The net effect is an overall cooling at the very same level that the K-F scheme was applying the greatest thermal forcing. This cooling effect is seen in Fig. 19b between 30 and 40 minutes after convective initiation, corresponding to the time separating the initial bore and the inverse-bore. This correlation between the time separating bores and inverse-bores, and the time it takes the atmosphere to respond to the convective scheme forcing and cool the upper troposphere, is inescapable; it is found in every case examined. This process effectively "turns off" the thermal forcing, akin to the trigger generating the inverse-bore like feature produced by Nicholls et al. (1991a). Thus, the cooling response of the atmosphere to the initial thermal forcing initiates the inverse-bore.

3.6. The Advection of Convective Heating Regions

These results suggest that a potentially complex pattern of bores and inverse-bores may be produced by an actively translating convective system. If the advection of a group of grid points representing a CHR systematically turns on-and-off neighboring grid points as it changes position within the grid (Fig. 20), does this in effect turn on-and-off the thermal forcing applied at the perimeter of this region? And if so, can a single convective region of constant thermal forcing create ripples of bores and inverse-bores simply by advecting? When determining when and where to initiate convection, the K-F scheme does take advection into account. If it is

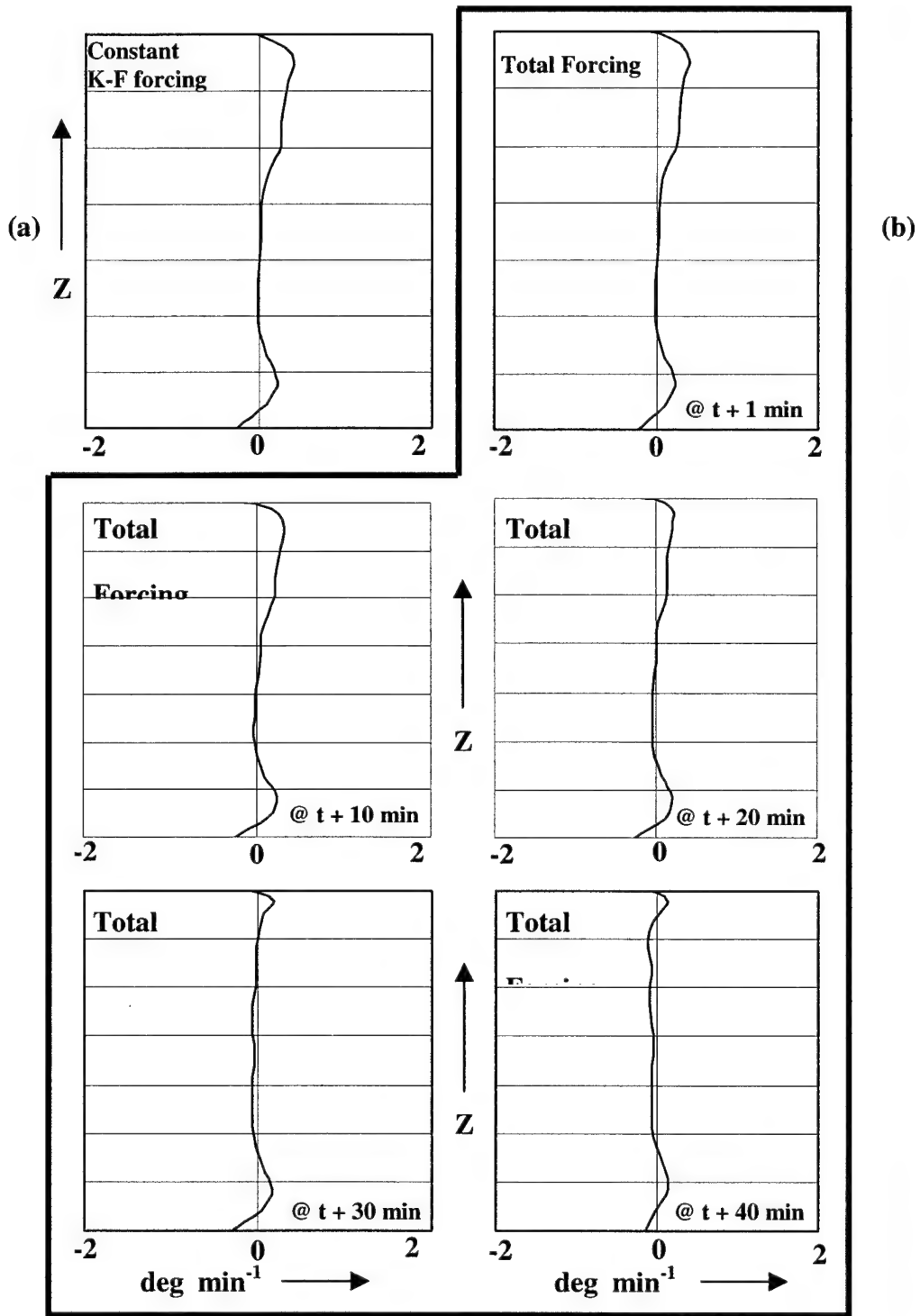


Fig. 19. (a) Vertical profile of continuous thermal forcing as dictated by the K-F convective parameterization scheme. Units are deg min^{-1} . (b) Time series of the atmospheric heating rate at a given time resulting from the cumulative effect of the thermal forcing applied in (a) and atmospheric response. t is the initiation time of thermal forcing by the K-F scheme.

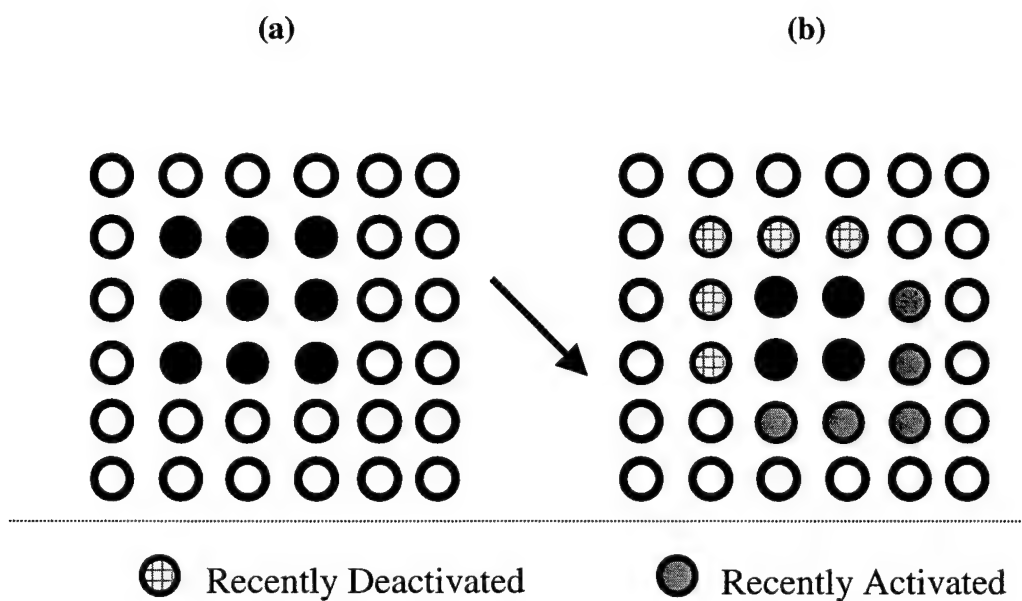


Fig. 20. The advection of a convective heating region across a model grid. Empty circles are inactive grid points. (a) The initial location of the convective heating region (black circles). (b) The convective heating region is advected one grid point southeast.

determined that conditions are sufficient to move convection from a currently active grid point to a non-active one, the scheme applies its thermal forcing profile to the once dormant grid point. Similarly, at the trailing edge of a convectively active region, the convective forcing at a grid point may be terminated once the environment is stabilized.

A modification of the K-F scheme allows for the manual advection of a simulated CHR. The vertical heating profile is kept constant to insure that any initiation or termination of thermal forcing is due solely to the advection of the region. The advection is applied to every convectively active grid point, with different advection rates explored. The entire CHR is advected one grid point in the same direction for three different time intervals: 24, 60, and 90 minutes.

The model reveals no bore or inverse-bore generation due to advection of the CHR (Fig. 21). The only bore/inverse-bore pairing that is generated is from the initial activation of the CHR. It is hypothesized that the time it takes a region to translate due to advection may allow for the atmosphere to sufficiently modify the environment adjacent to the CHR to a point that the initiation/termination of thermal forcing at those points no longer results in bore activity. However, as a convective region moves into different environments, with different heating profiles, it is possible that new bores may still be produced.

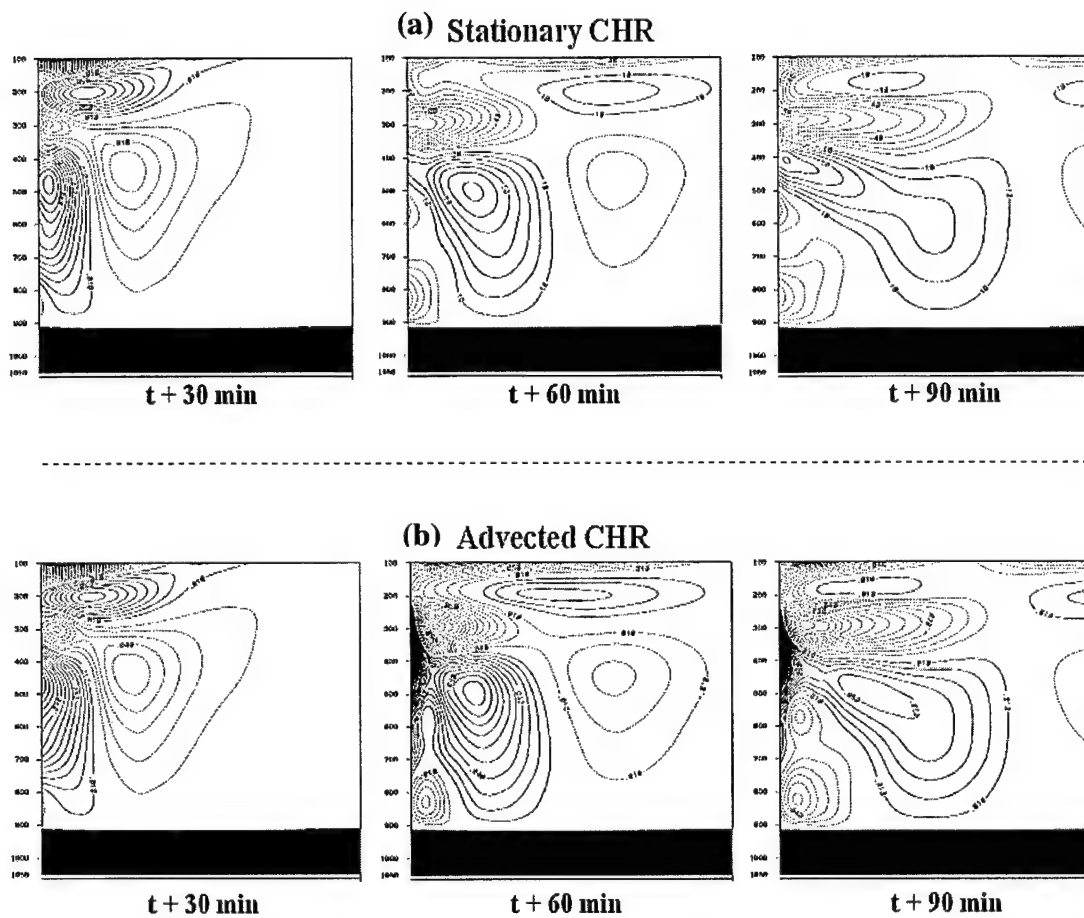


Fig. 21. Vertical cross-sections of vertical velocity. Units in m s^{-1} . Contour interval of 5 cm s^{-1} . The convective heating region is activated near the left edge of the cross-section and is (a) stationary; (b) allowed to advect one grid point after 24 minutes.

CHAPTER 4 – BORE BEHAVIOR IN A CONVECTIVE OUTBREAK

The information gathered on buoyancy bore behavior within the MM5 provides the tools necessary to examine buoyancy bore behavior in a more realistic, evolving, convectively active environment. This is motivated by the consideration that clouds are rarely isolated, and the vertical motions resulting from their convective initiation are usually a superposition of all the gravity-wave like forcing by all the clouds in the immediate region (Bretherton and Smolarkiewicz 1989). The convective outbreak on 23-24 June 1985, mentioned in Chapter 1, is again selected for the study. On this day, outflow boundaries from two different MCSs collided in central Kansas. Although new convection was forecast to develop, convective activity was not produced in the convergence zone. Stensrud and Maddox (1988) document that there was too much mid- to upper-level subsidence over the convergence zone, which acted to suppress convection. An examination is conducted to see if this subsidence can in any way be attributed to the buoyancy bores generated during this outbreak. For more details of this outbreak, see Stensrud and Maddox (1988).

There are two general observations of particular interest. The first is a cloud free environment separating the two convective systems (Fig. 22). The MCSs began forming in the northwest quadrant of Kansas near 2300 UTC 23 June. They maintained their intensity until roughly 0430 UTC 24 June, after which they began to weaken (Fig. 22). Throughout this time, the cloud free environment between them persisted. Due to the proximity and similarity in convective initiation times of the two systems, the most intense bore-related subsidence should be found in the cloud free

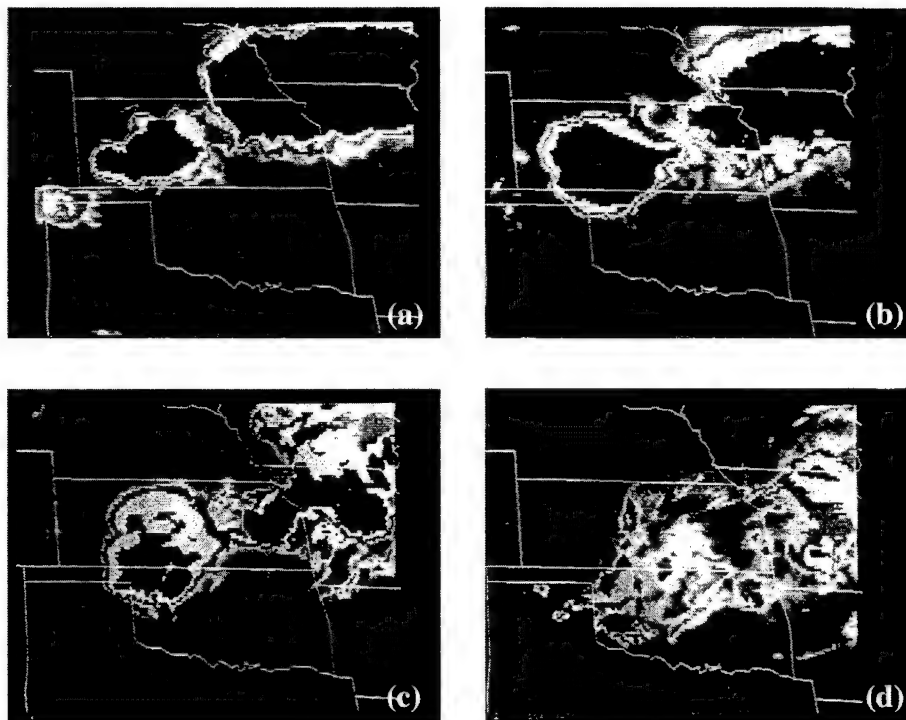


Fig. 22. Infrared satellite images taken at (a) 0200, (b) 0430, (c) 0600 and (d) 0900 UTC 24 June 1985. Enhancement indicates cloud top temperatures from -34° to -42° C as medium gray, -42° to -50° C as light gray, -50° -63° C a dark gray, and less than -63° C as black (from Stensrud and Maddox 1988).

environment separating the two. After exploring bore interactions between neighboring CHRs in a more idealized simulation, it is of interest to see if there are any visible effects of the complex pattern of overlapping bores and inverse-bores resulting from a continuously evolving convective event. The other observation of interest is the persistent interaction of the two outflow boundaries in central Kansas (Fig. 23). This interaction produces sustained low-level forcing for upward motion in a conditionally unstable environment, yet no new convection developed.

4.1. Developing the Convective Simulation

To simulate this event, the model is started from initial conditions valid at 1200 UTC 23 June. However, unlike the previous idealized experiments in which convection was forced to activate, in this run, the K-F scheme is allowed to behave as designed. Results show that the MM5 handled the convection rather poorly. A comparison between the MM5-generated convective pattern at 2000 UTC 23 June 1985, eight hours after the start of the run, and the national radar composite near that time shows that the convection in Kansas and Oklahoma is overstated (Fig. 24). Observations indicate that the convection in that area initiated at roughly 2200 UTC 23, two hours later than the model simulation. Since our focus is to include the cumulative effects of bores generated by convection at some distance away, the timing and location of convective initiation must be representative of the actual event. Thus, a more realistic representation of when and where convection initiated that day is needed if a fair estimation of the buoyancy bore pattern resulting from this convection is to be obtained. To that end, procedures similar to those described in

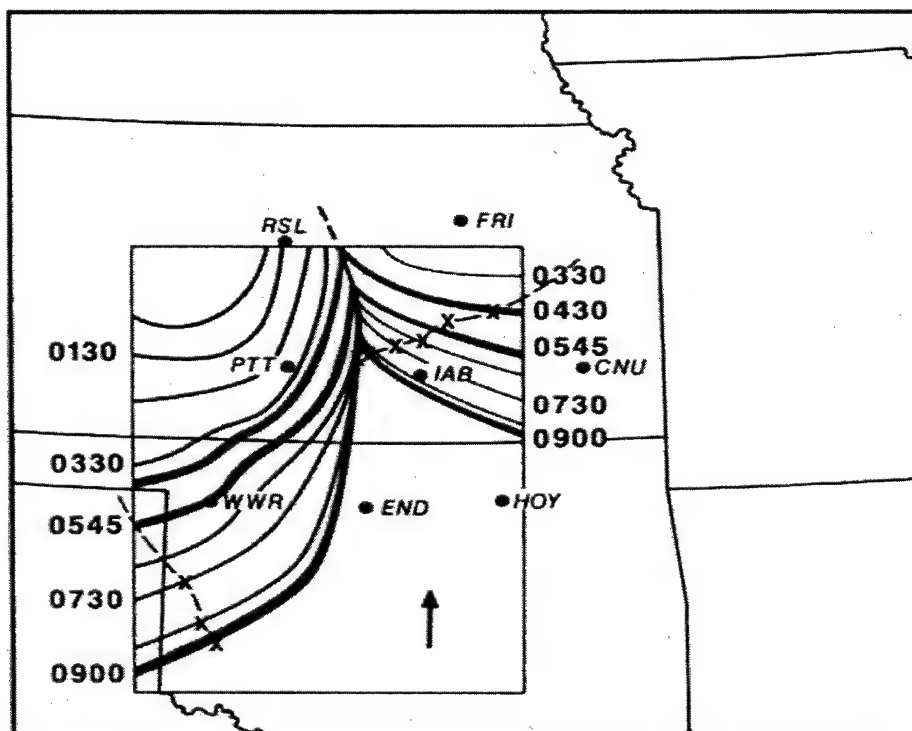


Fig. 23. Time progression of two outflow boundaries beginning at 0030 UTC 24 June 1985. The X denotes location of convergence maximum (from Stensrud and Maddox 1988).

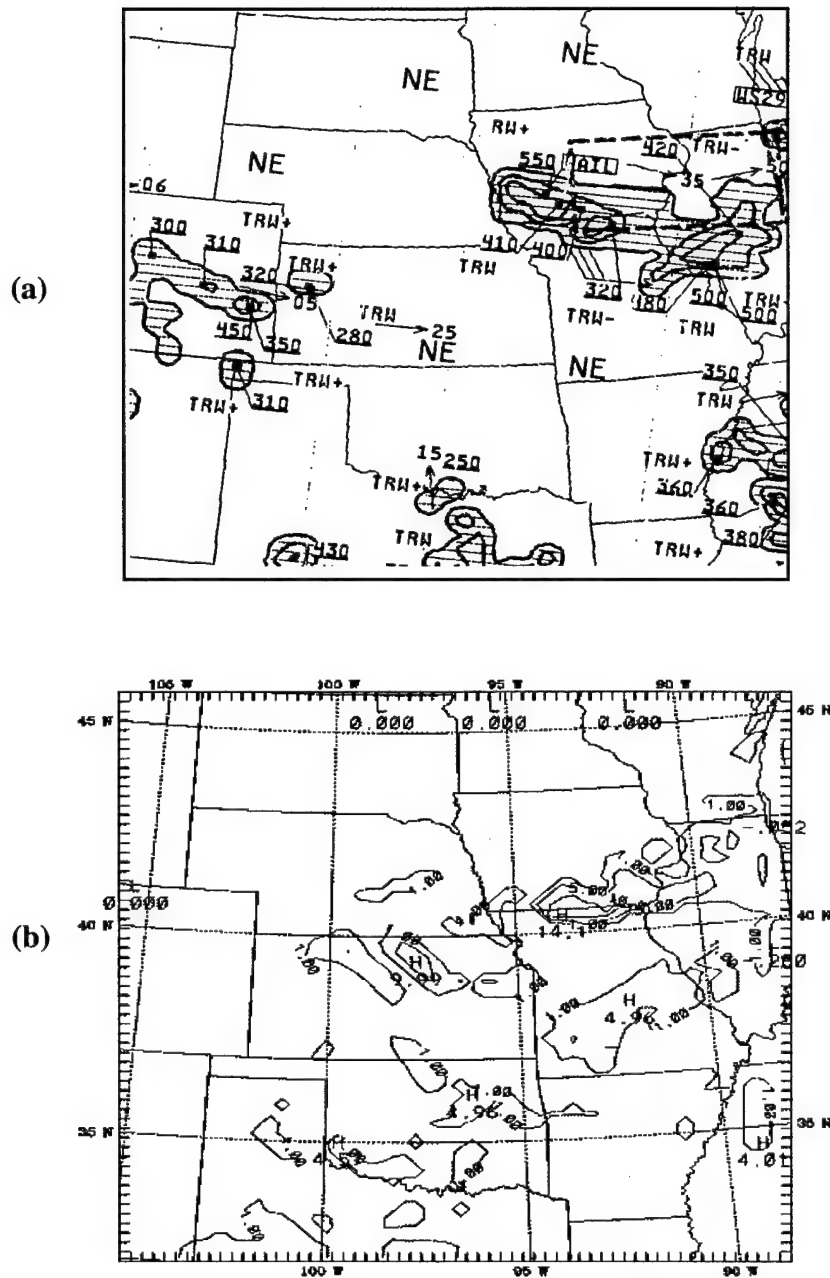


Fig. 24. A comparison of the (a) radar reflectivity summary at 1935 UTC 24 Jun 1985 and the (b) total hourly rain tendency at 2000 UTC the same day, as simulated by the MM5 mesoscale model with units of mm hr^{-1} .

Chapter 2 are used to force convection to develop in agreement with the observations.

In order to reflect the transient nature of the convective cells, additional time-dependent terms are included in the K-F scheme to force convection. By examining radar composites of the event, a template of the specific grid points that need to be activated at a particular time is created. Only those grid points with observed convective activity are activated; the other points are forced to remain inactive. With this technique, a much more accurate convective pattern is manufactured (Fig. 25). This allows for a reasonable portrayal of the location and timing of convection for the entire 24 hr period. The forced convection method likely can lead to some unrealistic atmospheric profiles due to forcing and suppressing convection in places where the model normally would not. However, since this does not appreciably affect when or where bores are initiated, it does not influence the results of this study. Unlike the more idealized model runs, here we view the full magnitudes of the fields, not just the perturbations. Also, in order to accurately portray the sequence of convective initiation for that time period, convective parameterization is forced on both grid-2 and grid-3. The grid-to-grid interactions due to convection may affect the ability to isolate bores, but this is unavoidable if we want to accurately recreate that day's pattern of convective initiation over a large region.

4.2 Behavior in an Area Separating Neighboring MCSs

Examination of cross sections of vertical velocity initiating at 2300 UTC within the cloud free region between the two MCSs (see Fig. 25) reveals typical mode-1 bore behavior (Fig. 26). The patterns are similar to CHR pairings in Chapter 3.

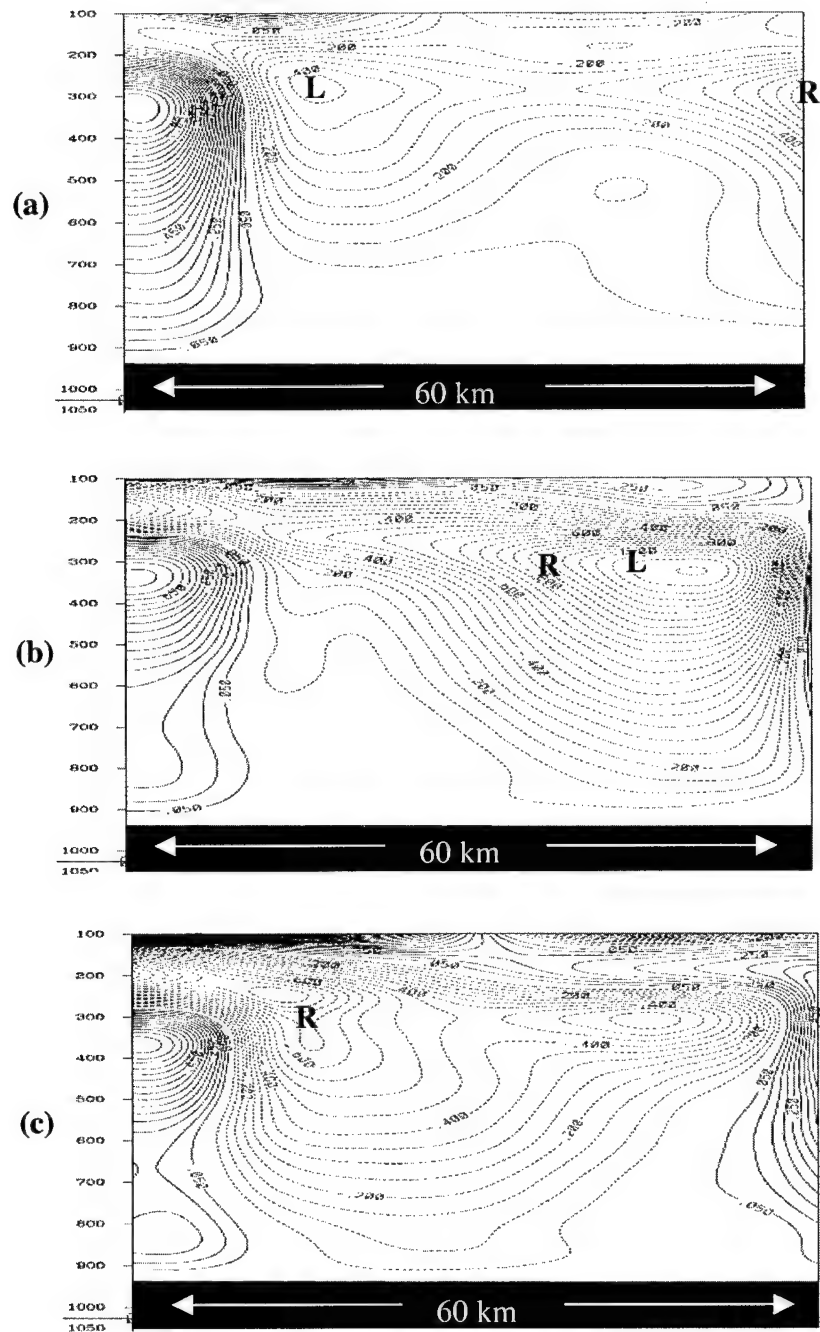


Fig. 26. Vertical cross section of vertical velocity, beginning at 2300 UTC. Units are as in Fig. 13. Thermal forcing is applied at the left and right boundaries. Time separating (a) from (b), and (b) from (c) is each 15 minutes. **L** is the mode-1 bore leaving from the left-most heat source, and **R** is the mode-1 bore leaving from the right-most heat source.

There are no indications of any complex patterns of bores and inverse-bores in association with the various CHRs surrounding the CHR-pairing being studied. The CHR on the left initiates 12 min before the one on the right. Shortly after convective initiation, the two bores overlap to temporarily form a region with maximum subsidence of 1.15 m s^{-1} just below the 300 hPa level (Fig. 26b). Note that this subsidence maximum is slightly to the right of the region that the two bores share. By 2330 UTC, analysis indicates that because of its earlier initiation, the bore from the leftmost CHR has propagated beyond the right edge of the cross-section, while the bore from the rightmost CHR has yet to reach the other CHR on the left (Fig. 26c). Notice that the subsidence maximum identified earlier (Fig. 26b) still has not moved in 15 minutes (Fig. 26c). Further investigation reveals that this stationary feature is not associated with a bore. It instead results from the convergence of storm-top outflow. Prior to the initiation of the two CHRs, the 250 hPa horizontal wind pattern is fairly laminar in the area of the cross-section (Fig. 27a). Shortly after the activation of the two CHRs, the resultant storm-top outflows begin to converge and continue to do so throughout the lifecycle of the simulated storms (Figs. 27b and 27c). The resultant convergence persists long after the bores have exited the area (Fig. 28). Even though this suggests that the maximum subsidence seen in Fig. 26b is not due solely to bores, the values seen will still be thought of as representative of an extreme case of bore-related subsidence.

Now that the existence and behavior of the bores has been identified, a closer examination of the subsidence attributed to them is conducted. A time series of a sounding at the location where the two bores overlap is scrutinized. First off, it is

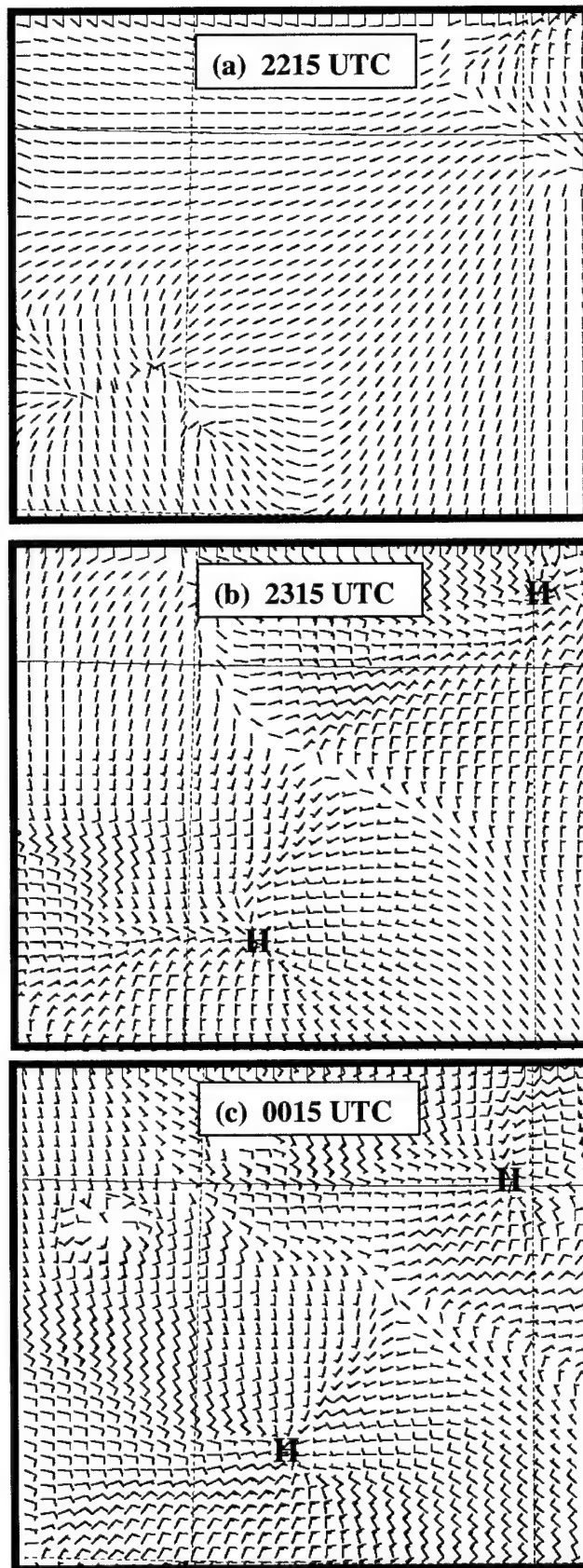


Fig. 27. Perturbation horizontal winds at 250 hPa, units in ms^{-1} . The letter **H** represents the centers of convective heating regions. Fields taken at (a) just before, (b) just after, and (c) over an hour after the initiation of thermal forcing.

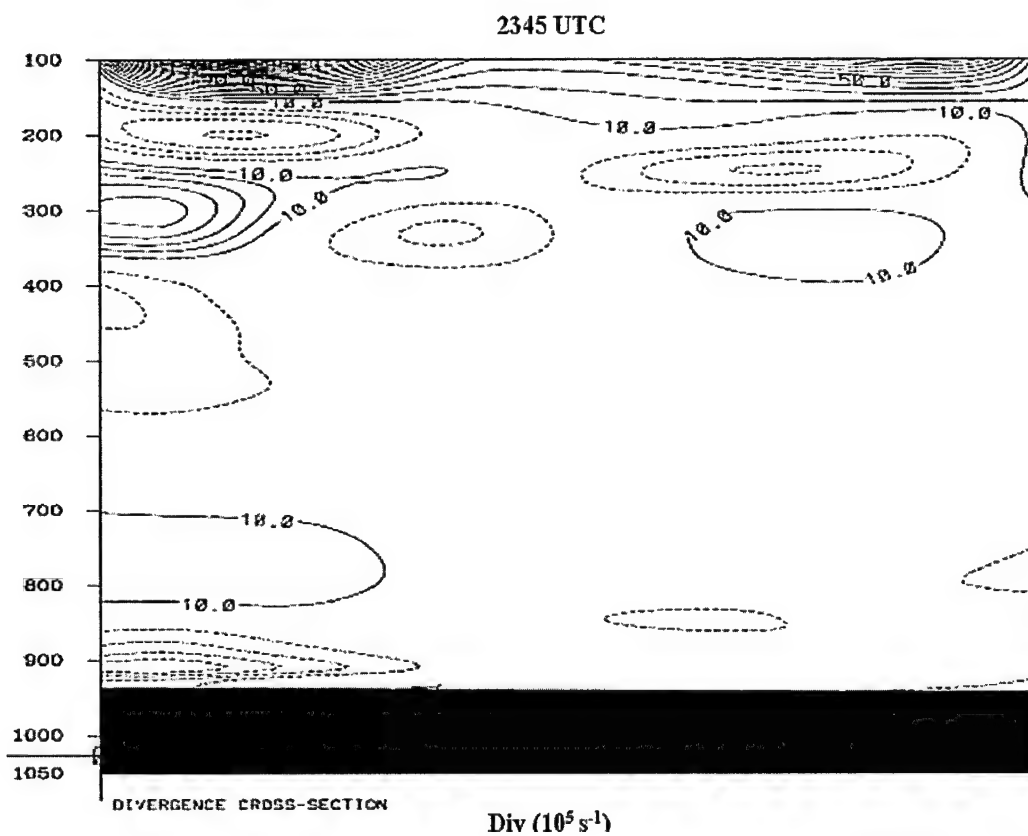


Fig. 28. Vertical cross-section of divergence taken between two convective heating regions. Note the area of upper-level convergence near 250 hPa in the right half of the cross-section. The feature persists well beyond buoyancy bore passage.

very noticeable that the atmosphere has become more moist above 300 hPa (Fig. 29). An examination of the integrated cloud water content suggests it is likely that the increase in moisture at that level is attributed to the advection of cirrus into the column. Aside from the cirrus advecting in above 300 hPa, the evolution of the upper troposphere indicates subsidence warming, but only down to the 600 hPa level. From 600 to just below 800 hPa, there is no apparent subsidence occurring. But subsidence again occurs down to the surface from 800 hPa. The effects of subsidence continue to dry the surface layer even after the bores have propagated out of the area. The persistence of low-level subsidence suggests that a process separate from the upper tropospheric bores might be responsible for the near-surface subsidence. Analysis of the horizontal wind, tangential to the plane of the cross-section, reveals convergent flow at 800 hPa at 30 minutes after the initiation of convection. The resulting convergence is weak initially (Fig. 30a). The convergence at this level increases three-fold 15 minutes later (Fig. 30b). An hour after convective initiation, the convergence at 800 hPa has yet to decrease in intensity (Fig. 30c). This flow is uncharacteristic of mode-1 buoyancy bores, since it is stationary and persists well beyond the timeframe associated with the bores. Analyzing other fields yields no additional evidence to suggest that the bores are responsible for the subsidence beneath 800 hPa.

4.3. Behavior in an Area Further Removed From MCSs

In the second area of interest, the region of convergent outflow boundaries in central Kansas (Fig. 23), vertical cross-sections are once again utilized. Because it is

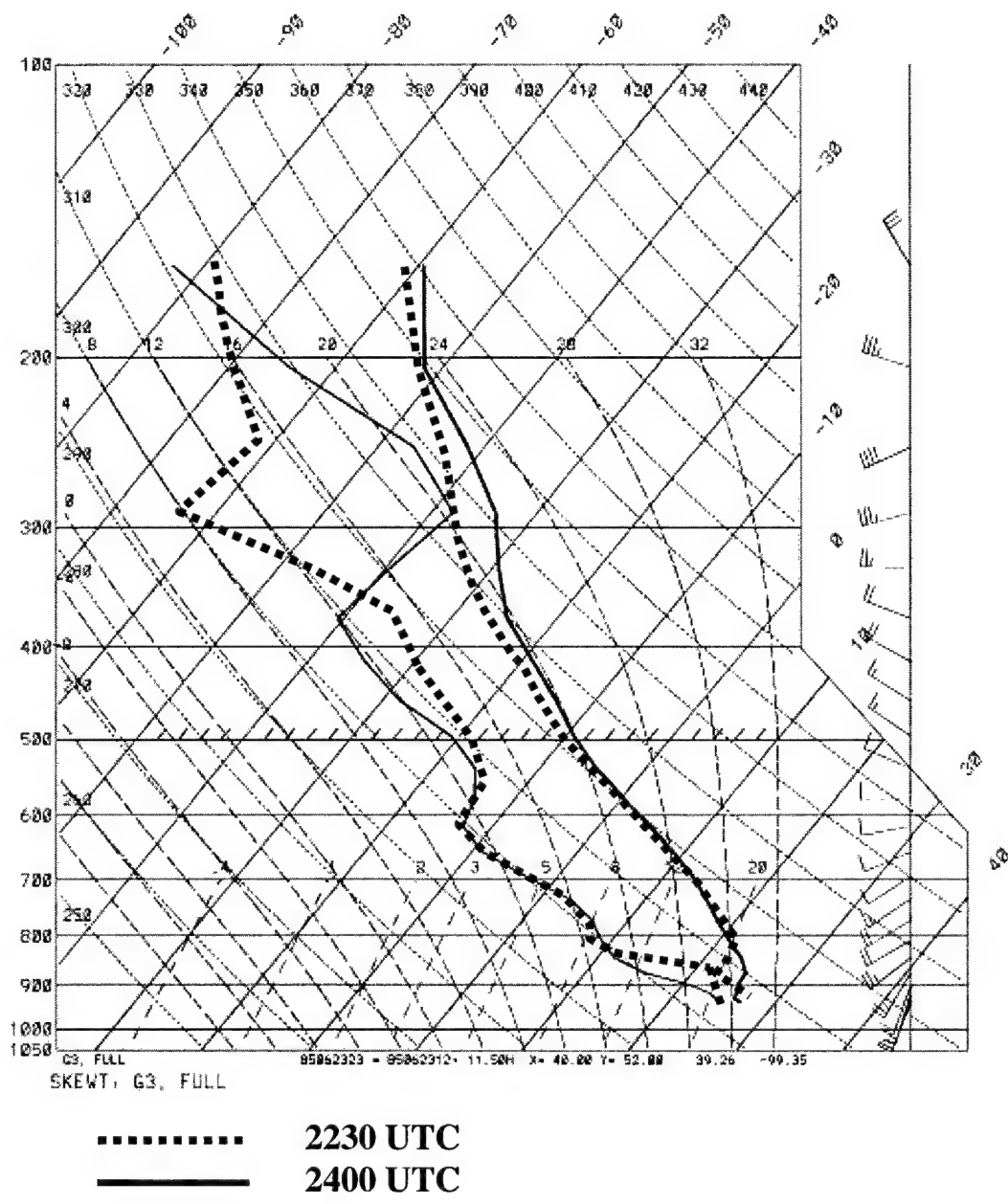


Fig. 29. Skew-T log-p of temperature and dewpoint from an environment separating two neighboring convective heating regions. The 'dashed' profile is taken prior to convective initiation. The 'solid' profile is of the environment approximately 15 min after the coincident passage of the mode-1 bores from each convective heating region.

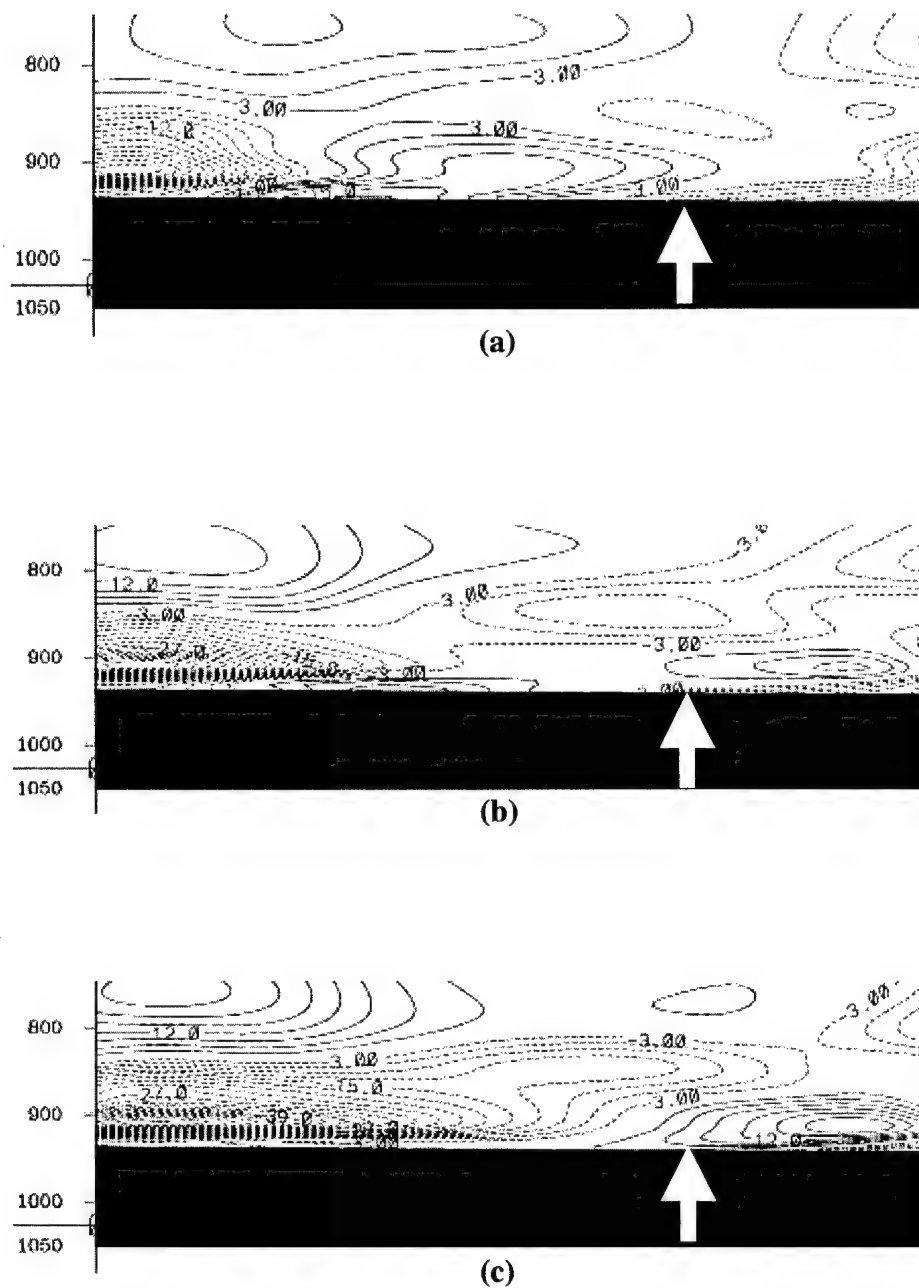


Fig. 30. Cross-sections of horizontal divergence in units of 10^5 s^{-1} , taken between two convective heating regions. The white arrows indicate the location from which the sounding in Fig. 26 was taken. The images are from (a) 2330, (b) 2345, and (c) 2400 UTC.

not surrounded by CHRs, bore passage through this cross-section is much weaker than was seen in the CHR-pairing simulation (Fig. 31). There is very little subsidence associated with these distant, partially dispersed bores. When subsidence is found, it is confined to the most upper regions of the troposphere. As with the first area examined, extensive interrogation reveals no evidence of any appreciable modification to the lower troposphere attributed to buoyancy bore subsidence.

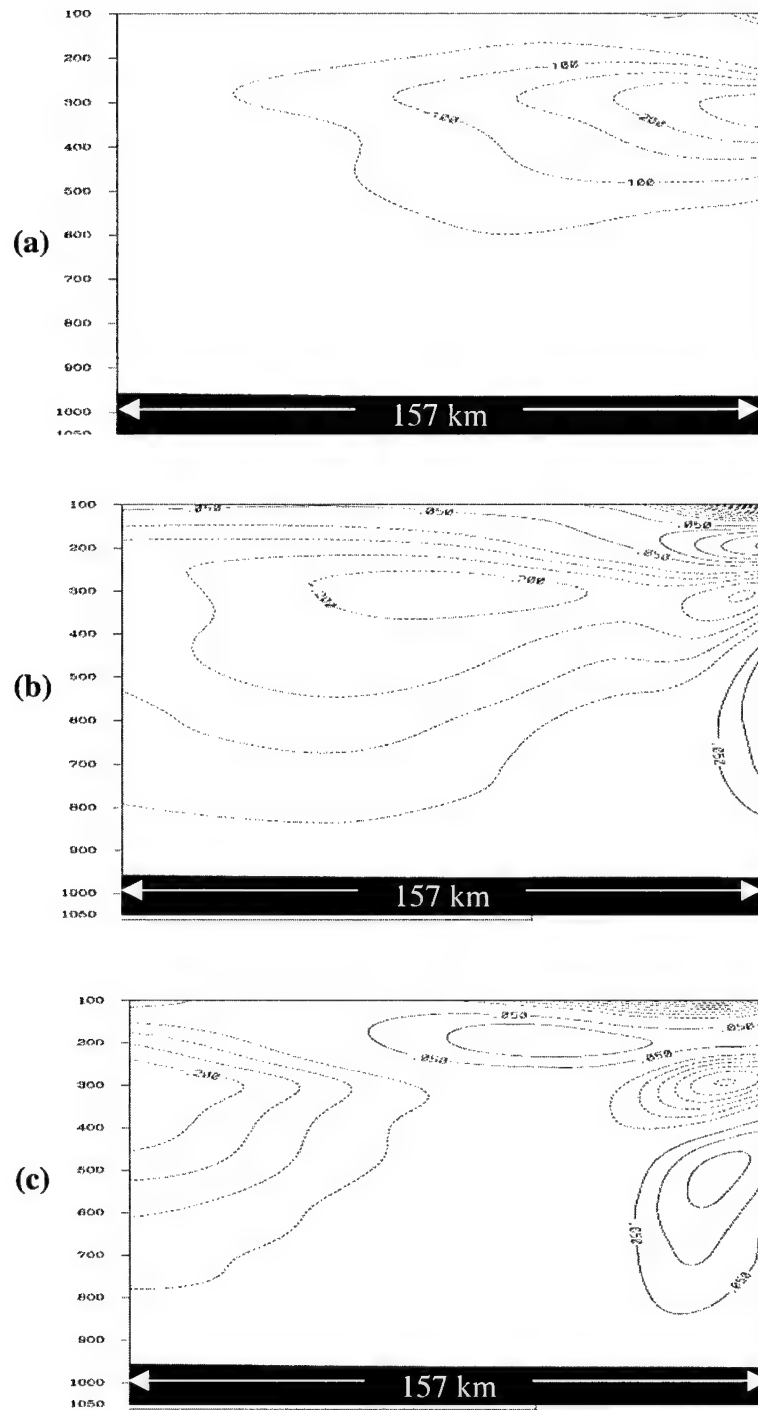


Fig. 31. Vertical cross section of vertical velocity. Units are as in Fig. 13. The time series of mode-1 buoyancy bore propagation is from (a) 2300, (b) 2330, and (c) 0000 UTC.

CHAPTER 5 - CONCLUSIONS

Upper-tropospheric subsidence, thought to be associated with gravity-wave like features resulting from deep convection, has been observed in the real atmosphere. By approximating the vertical profile of thermal forcing associated with convection, this subsidence has been replicated in numerical models. Model simulations of this type have shown that this subsidence is related to circulations induced by the non-periodic buoyancy bores that result from thermal forcing. Referencing such simulations, it has been suggested that mode-1 buoyancy bores alone can induce the mid- to lower-tropospheric subsidence often seen maintaining low-level inversions in areas separating neighboring MCSs, and this subsidence is capable of suppressing vertical ascent despite convergence at the surface. Other studies focus on the mode-2 bore's ability to enhance low-level convergence near MCSs, contributing to the production of convection. Through an examination of buoyancy bore behavior in a mesoscale atmospheric model, this paper explores these theories.

Through simulations of isolated and paired CHRs, the behaviors of buoyancy bores produced as a result of thermal forcing due to convection are isolated. The mode-1 bore is a dominant feature in the vertical velocity field. It originates within the CHR upon initiation. The magnitude of these bores is proportional to the amount of thermal forcing, but inversely proportional to the time they are active; they decay as they propagate. As bores propagating from two different CHRs meet, the upper-tropospheric subsidence at that point becomes the additive subsidence of the two bores. It is shown here that the maximum amount of mode-1 bore-related

subsidence is achieved within the area separating two CHRs as the bores from each overlap. The shorter the distance between the CHRs, the less the bores decay before they meet. As the bores continue their propagation, their properties remain unchanged by the overlap. It is important to note that mode-1 bores are concentrated at the level of maximum thermal forcing. As is characteristic of midlatitude MCSs, this is in the upper troposphere. Therefore, the subsidence accompanying these bores is far removed from the surface layer.

The atmospheric response of the MM5 to the positive thermal forcing applied by the CPS is to cool the upper troposphere. This response in effect turns off the positive thermal forcing initially induced by the convective scheme, producing another very significant feature -- the inverse-bore. Being generated later, it lags behind the mode-1 bore. It is of similar magnitude but results in upward vertical motion. This of course does not add to the production of subsidence between neighboring MCSs; this can only work to counteract the subsidence induced by the mode-1 bore as it moves through the same region.

Inverse-bores also are likely to affect the near-storm region where mode-2 bores are thought to enhance surface convergence. In an idealized model, with no atmospheric cooling in response to the constant thermal forcing, flow at the low-levels of the atmosphere is from the base of the faster-moving mode-1 bore into the base of the slower-moving mode-2 bore. In this setting, there are no inverse-bores. Low-level convergence is produced beneath the mode-2 bore, enhancing lift in the lower-levels of the atmosphere near MCSs. But when the atmosphere responds to the applied thermal forcing from convection, the mode-2 bore is not produced. The

inverse-bore disrupts this circulation. Due to its location between the mode-1 and mode-2 bores, the lower-level outflow from the mode-1 bore is ingested into the inverse-bore, presumably cutting off flow to the mode-2 bore. Unable to isolate any features that could be attributed to mode-2 bores, this paper concentrates on the mode-1 bores' contribution to low-level subsidence.

It is shown that, although substantial, the subsidence related to mode-1 bores is concentrated too far aloft to result in any atmospheric modifications in the lower atmosphere. Even when enhanced by storm outflow convergence aloft, the subsidence fails to modify the atmospheric temperature or dewpoint below 600 hPa. Considering the vertical profile of thermal forcing prevalent in these simulations, there is no reason to suggest that mode-1 buoyancy bores can effectively modify the lower troposphere to suppress convection in areas of low-level convergence on this day.

5.1. Additional Considerations

Early in this paper it is mentioned that another theory for the cause of subsidence sometimes reaching the lower levels of the troposphere is that it is created as a result of converging storm-top outflows. Care should be taken to not draw conclusions about this possibility based on findings in this paper. Any upper-atmospheric convergence between CHRs should not be regarded as representative of normal conditions. The modifications made to the model to force and suppress convection may result in unrealistic updrafts within the CHRs. These modifications do not significantly affect the study of bores, but properties of the updraft could result

in storm outflows aloft that may not be representative of what could be found in the naturally occurring environment.

The vertical profiles of thermal forcing recurring throughout the simulations studied in this paper are representative of what is typically observed in midlatitude MCSs. Although it has been shown that thermal forcing profiles of tropical cloud clusters can have structures similar to midlatitude MCSs, the parameterization of this tropical convection can lead to a much different profile (Kain and Fritsch 1990). By using a cloud model that allows for a more physically realistic variation in the detrainment and entrainment of individual updraft supercells (Variable E/D), the CPS produces a profile differing significantly from models using less sophisticated calculations of entrainment (Fig. 32). A cloud model maximizing heating in the lower troposphere would likely result in mode-1 bores that propagate through the lower troposphere. The resulting low-level subsidence would likely yield results and conclusion contrasting with what is presented in this paper. Therefore, as increased computing power provides us the ability to employ more sophisticated models, care must be taken to ensure that the vertical profiles of thermal forcing generated by CPSs are representative of observations. The sensitivity of the results of this paper to the vertical profile of thermal forcing cannot be overemphasized.

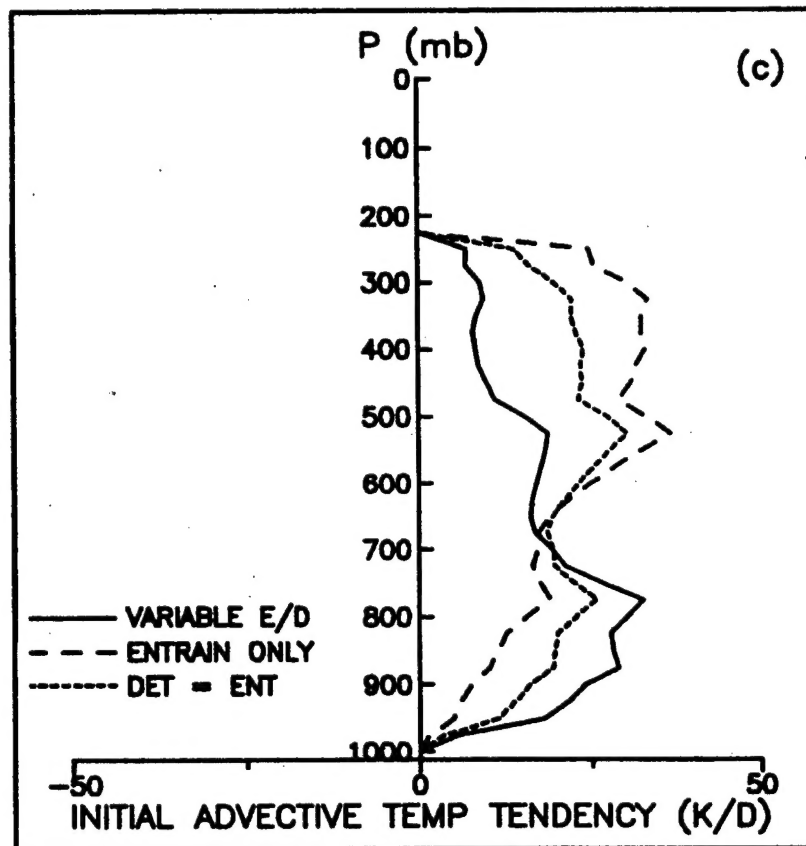


Fig. 32. Vertical profile of thermal forcing from the Fritsch-Chappell CPS using various cloud models. The entrainment/detrainment is handled differently within each cloud model resulting in different profiles. From Kain and Fritsch (1990).

REFERENCES

- Benjamin, S. O., and N. L. Seaman, 1985: a simple scheme for objective analysis in curved flow. *Mon. Wea. Rev.*, **113**, 1184–1198.
- Braun, S. A., and W. K. Tao, 2000: Sensitivity of high-resolution simulations of Hurricane Bob (1991) to planetary boundary layer parameterizations. *Mon. Wea. Rev.*, **128**, 3941–3961.
- Bretherton, C. S., and P. K. Smolarkiewicz, 1989: Gravity waves, compensating subsidence and detrainment around cumulus clouds. *J. Atmos. Sci.*, **46**, 740–759.
- Burk, S. D., and W. T. Thompson, 1989: A vertically nested regional numerical weather prediction model with second-order closure physics. *Mon. Wea. Rev.*, **117**, 2305–2324.
- Deardorff, J. W., 1977: A parameterization of the ground surface moisture content for use in atmospheric prediction models. *J. Appl. Meteor.*, **16**, 1182–1185.
- Dudhia, J., 1993: A nonhydrostatic version of the Penn State-NCAR Mesoscale Model: Validation tests and simulation of an Atlantic cyclone and cold front. *Mon. Wea. Rev.*, **125**, 1493–1513.
- Gallus, W. A., Jr., and R. H. Johnson, 1991: Heat and moisture budgets of an intense midlatitude squall line. *J. Atmos. Sci.*, **48**, 126–146.
- Grell, G. A., J. Dudhia and D. R. Stauffer, 1994: A description of the fifth generation Penn State/NCAR Mesoscale Model (MM5). NCAR Tech. Note NCAR/TN 398+STR, 138 pp.
- Haertel, P. T., and R. H. Johnson, 1999: The linear dynamics of squall line mesohighs and wake lows. *J. Atmos. Sci.*, **50**, 2026–2037.
- Houze, R. A., Jr., 1982: Cloud clusters and large-scale vertical motions in the tropics. *J. Meteor. Soc. Japan*, **60**, 396–410.
- Johnson, R. H., and G. S. Young, 1983: Heat and moisture budgets of tropical mesoscale anvil clouds. *J. Atmos. Sci.*, **40**, 2138–2147.
- _____, B. D. Miner and P. E. Ciesielski, 1995: Circulations between mesoscale convective systems along a cold front. *Mon. Wea. Rev.*, **123**, 585–599.

- Kain, J. S., and J. M. Fritsch, 1990: A one-dimensional entraining/detraining plume model and its application in convective parameterization. *J. Atmos. Sci.*, **47**, 2784-2802.
- Knupp, K. R., B. Geerts and S. J. Goodman, 1998: Analysis of a small, vigorous mesoscale convective system in a low-shear environment. Part I: formation, radar echo structure, and lightning behavior. *Mon. Wea. Rev.*, **126**, 1812-1836.
- Lin, Y. L., and R. C. Goff, 1988: A study of a mesoscale solitary wave in the atmosphere originating near a region of deep convection. *J. Atmos. Sci.*, **45**, 194-205.
- Mapes, B. E., 1993: Gregarious tropical convection. *J. Atmos. Sci.*, **50**, 2026-2037.
- Nicholls, M. E., R. A. Pielke and W. R. Cotton, 1991a: Thermally forced gravity waves in an atmosphere at rest. *J. Atmos. Sci.*, **48**, 1869-1884.
- _____, _____ and _____, 1991b: A two-dimensional numerical investigation of the interaction between sea breezes and deep convection over the Florida peninsula. *Monthly Weather Review*, **119**, 298-323.
- Ogura, Y., and M. T. Liou, 1980: The structure of a midlatitude squall line. *J. Atmos. Sci.*, **37**, 553-567.
- Pandya, R., and D. Durran 1996: The influence of convectively generated thermal forcing on the mesoscale circulation around squall lines. *J. Atmos. Sci.*, **53**, 2924-2951.
- _____, _____ and C. Bretherton, 1993: Comments on "Thermally Forced Gravity Waves in an Atmosphere at Rest". *J. Atmos. Sci.*, **50**, 4097-4101.
- Stensrud, D. J., and R. A. Maddox, 1988: Opposing mesoscale circulations: A Case Study. *Wea. Forecasting*, **3**, 189-204.
- Warner, T. T., and H. M. Hsu, 2000: Nested-model simulation of moist convection: The impact of coarse-grid parameterized convection on fine-grid resolved convection. *Mon. Wea. Rev.*, **128**, 2211-2231.
- Wu, X., 1993: Effects of cumulus ensemble and mesoscale stratiform clouds in midlatitude convective systems. *J. Atmos. Sci.*, **50**, 2496-2518.
- Xu, M., J. Bao, T. T. Warner, and D. J. Stensrud, 2001: Effect of time step size in MM5 simulations of a mesoscale convective system. *Mon. Wea. Rev.*, **129**, 502-

516.